Subarctic Thermokarst Ponds: Investigating Recent Landscape Evolution and Sediment Dynamics in Thawed Permafrost of Northern Québec (Canada)

Author(s): Frédéric Bouchard , Pierre Francus , Reinhard Pienitz , Isabelle Laurion and Stéphane Feyte

Subarctic Thermokarst Ponds: Investigating Recent Landscape Evolution and Sediment Dynamics in Thawed Permafrost of Northern Québec (Canada)

Frédéric Bouchard*†§

Pierre Francus*†

Reinhard Pienitz†‡

Isabelle Laurion*† and

Stéphane Feyte*

*Institut national de la recherche scientifique, Centre Eau Terre Environnement (INRS-ETE), 490 de la Couronne, Québec (QC), G1K 9A9, Canada

†Centre d'études nordiques (CEN), Pavillon Abitibi-Price, Université Laval, 2405 de la Terrasse, Québec (QC), G1V 0A6, Canada

‡Département de Géographie, Pavillon Abitibi-Price, Université Laval, 2405 de la Terrasse, Québec (QC), G1V 0A6, Canada

§Corresponding author (present address): Centre d'études nordiques (CEN), Pavillon Abitibi-Price, Université Laval, 2405 de la Terrasse, Québec (QC), G1V 0A6, Canada, frederic.bouchard@cen.ulaval.ca

Abstract

Although widely distributed throughout Arctic and subarctic regions, thermokarst ponds and lakes remain relatively unexplored regarding geomorphological changes in their catchments and their internal properties in relation to climate change over the past decades. This study synthesizes recent landscape evolution and modern sedimentology of limnologically diverse thermokarst ponds near southeastern Hudson Bay, Canada. Spatio-temporal analysis of permafrost mounds, thermokarst ponds, and vegetation surface areas over the past five decades revealed that the recent climate-induced decrease of permafrost-affected areas was not primarily compensated by thermokarst pond development, but rather by a remarkable increase in vegetation cover. These changes appeared to be modulated by topographical and hydrological gradients at the study site, which are associated with eastward increasing thickness of postglacial marine deposits. At a more contemporary time-scale, physico-chemical measurements made on sedimenting materials (sediment traps) and freshly deposited lacustrine sediments of selected thermokarst ponds revealed striking differences both among ponds and between the oxic epilimnion and the oxygen-depleted hypolimnion. These findings underscore the major influence of local landscape properties and oxycline development on pond sedimentology and geochemistry, such as the transport of detritic particles and the concentration of redox-sensitive elements.

Introduction

Thermokarst ponds and lakes are formed by local ground subsidence caused by the thawing and erosion of ice-rich permafrost. These aquatic ecosystems are widespread throughout Arctic and subarctic regions of northern Scandinavia (Zuidhoff and Kolstrup, 2000; Christensen et al., 2004), Siberia (Agafonov et al., 2004; Takakai et al., 2008), Alaska (Jorgenson et al., 2006; Osterkamp, 2007), and Canada (Beilman et al., 2001; Payette et al., 2004). Their stability and life cycle—from days to thousands of years—are strongly controlled by regional climate variations, as well as local factors such as hydrology and substrate properties (Pienitz et al., 2008). The surrounding landscape of thermokarst ponds generally contains significant amounts of organic carbon—formerly trapped in permafrost and now being mobilized with global warming and associated erosion—that can be partly mineralized to CO_2 and CH_4 in aquatic systems, and then transferred to the atmosphere (Zimov et al., 2006; Schuur et al., 2009; Tarnocai et al., 2009). Thermokarst systems thus contribute actively to greenhouse gas (GHG) emissions, potentially enhancing climate warming through a positive feedback mechanism and affecting the global carbon balance when old carbon is released (Walter et al., 2006; Schuur et al., 2008). It was proposed that the global atmospheric increase in CH_4 during the last deglaciation was directly related to this mechanism, although this subject is still under debate (Walter et al., 2007; van Huissteden et al., 2011; Brosius et al., 2012).

Covering about 25% of the northern hemisphere and more than 50% of Canada (Brown et al., 1998), permafrost spans nearly one-third of the northern Québec-Labrador peninsula, and a significant part (at its southern limit) is considered as *warm* permafrost, or near the thawing threshold (Allard and Seguin, 1987). Since the mid-20th century, increasing air/ground temperatures and snow cover along the eastern coast of Hudson Bay have contributed to the widespread reduction of permafrost areas along a latitudinal gradient, from about 25% in northern Hudson Bay (58°N; Vallée and Payette, 2007) to more than 80% in its southeastern part (56°N; Payette et al., 2004). Therefore, thermokarst ponds and lakes may occupy an increasingly important part of the landscape in subarctic Québec, although precise pond and lake surface areas are still unknown for this specific region. Smith et al. (2007) estimated that 73% of all lakes north of 45.5°N are located in permafrost-influenced zones, representing nearly 150,000 lakes with surface areas between 0.1 and 50 km². However, this number is likely underestimated as many northern ponds and lakes are generally <0.1 km², thus not included in large-scale surface classifications. This is of great importance for the global carbon balance, as small lakes and ponds (hundreds of m²) must also be regarded as effective processors and conduits of carbon in Arctic and boreal landscapes (Kortelainen et al., 2006; Abnizova et al., 2012; Negandhi et al., 2013).

Studies examining recent changes in the distribution and surface area of thermokarst ponds and lakes in Arctic and subarctic regions have reported contrasting trends according to permafrost types: water-level decline and pond/lake shrinkage in

the discontinuous zone and pond/lake expansion or no significant change in the continuous zone (Yoshikawa and Hinzman, 2003; Smith et al., 2005; Riordan et al., 2006; Plug et al., 2008; Carroll et al., 2011). Such differences in observations can be explained if thermokarst processes are considered as a continuum: initial permafrost thawing results in thermokarst lake inception and expansion, followed by a reduction of lake surface area to complete subsurface drainage as the permafrost warms and degrades further, allowing hydrological connections between surface and underground flows through portions of unfrozen ground (taliks) (Smith et al., 2005). Lateral drainage, caused by lakeshore breaching related to high water levels, has also been reported, even in the continuous permafrost zone (Jones et al., 2011). These landscape changes can have substantial impacts on the carbon-climate feedback: expanding ponds and lakes can act as net carbon sources when previously frozen organic carbon is mobilized to the atmosphere through aquatic processes (Walter et al., 2006; Laurion et al., 2010; Abnizova et al., 2012), whereas drained or shrinking water masses would rather act as net carbon sinks (at least for CO_2) when resumed vegetation development and peat accumulation proceed in the old lakebeds through terrestrialization (Payette et al., 2004; Arlen-Pouliot and Bhiry, 2005; van Huissteden et al., 2011). Thus, the *timing* of such landscape changes and their consequences on sediment erosion and redistribution within thermokarst systems are of critical importance for the evolution of biogeochemical cycles in the north. Despite the importance of these ubiquitous systems in a region facing large climate pressures, the complex links between recent landscape evolution (e.g., geomorphology and hydrology) and related internal thermokarst processes (e.g., sedimentology, geochemistry, and limnology) remain poorly known. Building on remote sensing, geophysical and modeling studies of permafrost-thermokarst-vegetation changes over the past ~5 decades in Scandinavia, Siberia, Alaska, and western/central Canada (Plug et al., 2008; Labrecque et al., 2009; Parsekian et al., 2011; Sannel and Kuhry, 2011), we aimed at filling the gap by adding new insights on sedimentological and geomorphological processes from the southern edge of the discontinuous permafrost zone in eastern Canada.

This study was part of a wider research program investigating thermokarst ponds in subarctic Québec (Breton et al., 2009; Laurion et al., 2010; Bouchard et al., 2011; Watanabe et al., 2011; Bouchard et al., 2013 Rossi et al., 2013). The overall objectives of the present study were (1) to quantify changes in permafrost, thermokarst ponds, and vegetation surface areas during the last ~50 years, and (2) to identify the main processes controlling sediment and chemical element dynamics in limnologically contrasting ponds through a complete annual cycle, including seasonal changes (e.g., stratification and mixing, ice-cover formation, and melting). In a broader perspective, it provided a synthesized model for subarctic thermokarst pond evolution in the recent past, building on lithostratigraphic (Bouchard et al., 2011) and biostratigraphic (Bouchard et al., 2013) work conducted on sediment cores at the same study site. This paper presents the results obtained within a delimited thermokarst pond area of ~25 hectares, focusing on six ponds with contrasting limnological properties (e.g., color, transparency, and dissolved and particulate component concentrations). The approach combined (1) aerial photographs and satellite imagery and (2) sediment trap and surface soil sampling. To our knowledge, this study is the first of its kind concerning recent evolution and sedimentological dynamics of subarctic thermokarst ponds derived from the thawing of permafrost mounds, thereby contributing to a growing literature on thermokarst landscape evolution.

Study Area

The study site (55°20′N, 77°30′W; 105 m a.s.l.) is located about 20 km inland from the southeastern coast of Hudson Bay, near the hamlet of Kuujjuarapik-Whapmagoostui in subarctic Québec (Fig. 1). It lies on Precambrian granitic/gneissic rocks strongly eroded by Pleistocene glaciations, the last one (Wisconsin) ending in the region around 8000 cal yr BP when the Laurentide Ice Sheet retreated northward and eastward (Dyke and Prest, 1987). Final break-up of the ice sheet triggered the rapid outburst of proglacial lake Agassiz-Ojibway (Barber et al., 1999; Lajeunesse and St-Onge, 2008) and the formation of the Late Glacial Sakami moraine (Hillaire-Marcel et al., 1981). This deglaciation was followed, around 7900 cal yr BP, by the postglacial transgression of the Tyrrell Sea (precursor of Hudson Bay), which submerged the landscape up to present-day elevations of 250–300 m a.s.l. and left thick deposits of marine silty clays and littoral sands in topographic depressions (Hillaire-Marcel, 1976; Saulnier-Talbot and Pienitz, 2001). Postglacial emergence of the area occurred at about 6000 cal yr BP and glacio-isostatic uplift has been estimated at more than 1 m per century (Allard and Tremblay, 1983; Lavoie et al., 2012).

The prevailing climate is subarctic. Mean annual air temperature at the Kuujjuarapik-Whapmagoostui weather station (55°17′N, 77°45′W; 10 m a.s.l.) is –4.4 °C, ranging from monthly means of –23.4 °C in January to 11.4 °C in August (Environment Canada, 2012a). The annual freezing index (sum of degree-days below zero) is 2890, more than twice the thawing index (sum of degree-days above zero), which is 1310. The mean frost-free period (minimum daily temperature >0 °C) is 126 days and the growing season extends from mid-May to the end of September. Annual precipitation is about 650 mm, with more than 35% falling as snow. Snow starts to accumulate on the ground in September-October, reaches a maximum depth (~40 cm) in March, and disappears at the end of May. During the last decades (since mid-1960s), the total annual precipitation has slightly and gradually increased, whereas the mean annual temperature has remained rather stable until the early 1990s when it started to increase sharply (Appendix Fig. A1). The study area lies at the southern edge of the discontinuous and scattered (also called sporadic) permafrost zone, where less than 50% of the land surface (mainly exposed hills and peatlands) is affected by permafrost (Allard and Seguin, 1987; Brown et al., 1998).

The study site is located in a small north-south-oriented thermokarst landscape covering about 0.5 km^2 (~1.0 km N–S × ~0.5 km E–W) and representative of the extensive permafrost peatlands that developed over silt-clay marine deposits along eastern Hudson Bay (Allard and Seguin, 1987; Payette, 2001; Payette et al., 2004), and that are now in an advanced state of degradation. The thawing of permafrost mounds has triggered the formation of several thermokarst ponds (Fig. 1), which are now mostly circular (10–30 m diameter) and shallow (1–3.5 m depth). In most cases, they are surrounded by a 1–2 m high peripheral ridge covered by shrubs and trees, some of them with also small areas of aquatic grass meadows. They are located in the upper section of a small glacial valley that gently slopes southward toward the Kwakwatanikapistikw River (local Cree name), a tributary of the Great Whale River. Although the landscape is relatively flat, slight topographic and hydrologic gradients extend from the west (adjacent rocky hills) to the east (steeply embedded creek). Based on former studies in the area (Arlen-Pouliot and Bhiry, 2005; Bhiry and Robert, 2006; Calmels et al., 2008a) and on sediment sampling of the peripheral ridges (this paper), it is assumed that the marine sediments between and underneath the ponds are permafrost-free. In
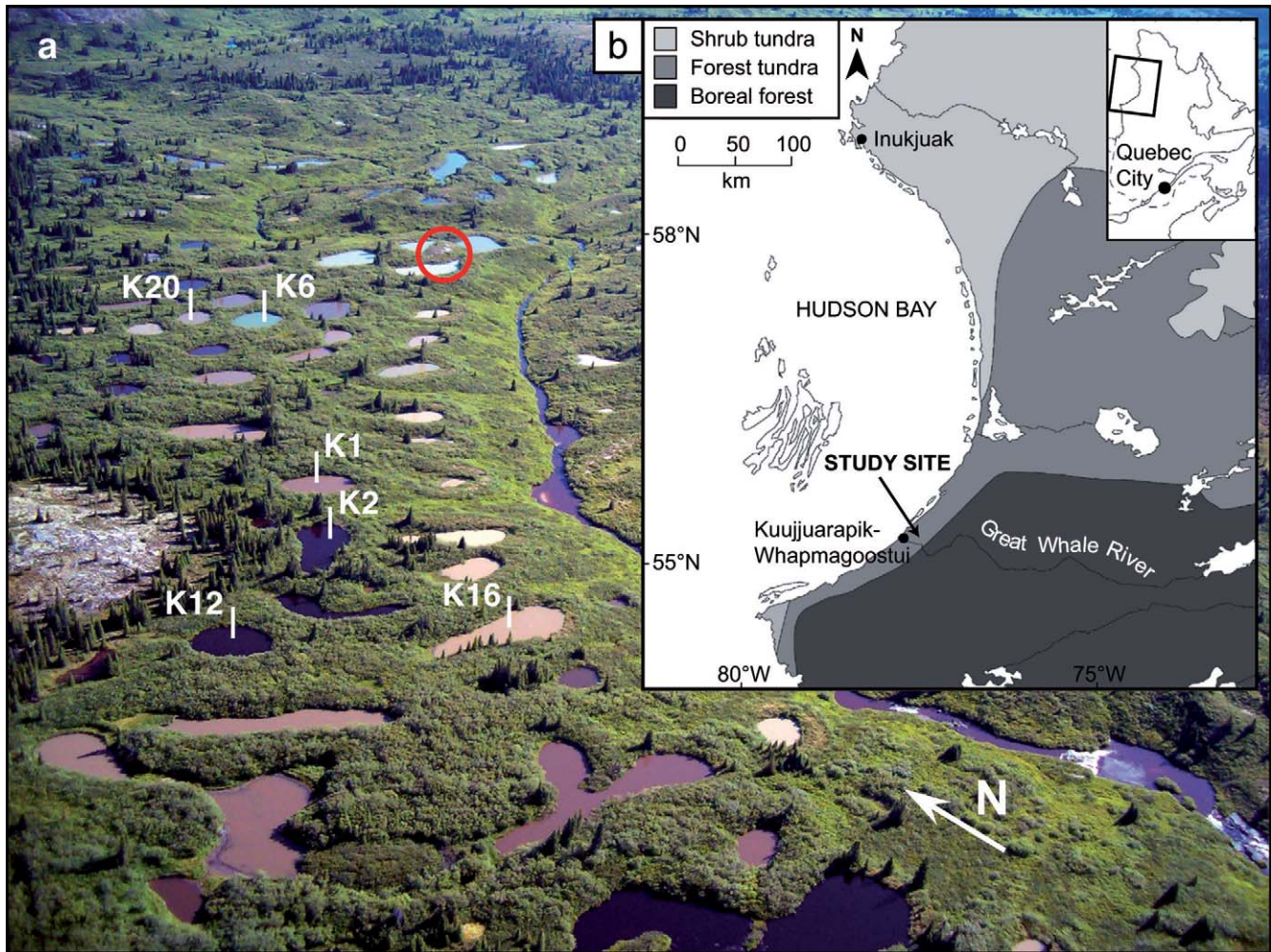
FIGURE 1. Location of the study site. (a) Oblique aerial photograph showing sampled ponds (numbers as in the text). The red circle shows the only permafrost mound (lithalsa) still present in the field. (b) Regional map showing the vegetation zones in subarctic Québec (modified from Arlen-Pouliot and Bhiry, 2005). The study site (55°20′N; 77°30′W) is located near Kuujjuarapik-Whapmagoostui, along the Great Whale River.

fact, only one mineral permafrost mound (lithalsa) is still visible on the site, and it is severely affected by thawing and surrounded by newly formed turbid thermokarst ponds (Figs. 1 and 3).

The vegetation cover in the region is typical of the forest-tundra zone in subarctic Québec (Payette and Bouchard, 2001). Sparse trees and shrubs (e.g., *Picea mariana*, *P. glauca*, *Larix laricina, Ledum groenlandicum, Betula glandulosa*) colonize peripheral ridges, whereas poorly drained soils between the ponds are mostly occupied by dense shrubs (*Salix* sp., *Alnus crispa*, *Myrica gale*), mosses (*Sphagnum* spp.), and herbaceous plants (e.g., *Carex aquatilis*). The studied ponds have strikingly different limnological properties (Table 1), including dissolved organic carbon (DOC) and total suspended solids (TSS) (for a detailed limnological description of these ponds and related methods see Breton et al., 2009; Laurion et al., 2010; and Watanabe et al., 2011). Most of them are relatively humic and nutrient-rich systems where dissolved organic matter (DOM) has a dominant allochthonous signature likely derived from thawing permafrost soils (Breton et al., 2009). Despite their shallow water depth, these ponds are characterized by low light availability (thus limited photosynthesis), remain seasonally stratified with a hypoxic/anoxic hypolimnion, and are considered heterotrophic systems with supersaturated concentrations of dissolved CO_2 and CH_4 (Laurion et al., 2010).

Methods

SPATIO-TEMPORAL ANALYSIS (REMOTE SENSING)

To quantify changes in permafrost, thermokarst, and vegetation surface areas over the past five decades, we used remote sensing data available for the study site, including aerial photographs from 1959 and a high-resolution satellite image from 2006. First, two adjacent black-and-white aerial photographs were acquired from La Géomathèque (Québec, QC, Canada). These photographs were taken on 7 July 1959 at a flight elevation of ~4800 m. With an original scale of half a mile per inch (1: 31,680), they were scanned (TIFF format) at 1814 dpi resolution, which provided a pixel size of 44 cm on the ground. Second, a panchromatic (450–900 nm) QuickBird scene was acquired from DigitalGlobe (Longmont, CO, U.S.A.). This satellite image was taken on 7 July 2006 under cloud-

TABLE 1

Morphology, limnology, and type of analyses conducted in sampled ponds.

		Pond #								
		K1	K2	K6	K12	K16	K20	Min	Max	Mean
		brown	black	blue-green	black	beige	beige			
General morphology										
Max depth	m	2.3	3.0	3.5	2.7	2.5	2.7	2.3	3.5	2.7
Secchi depth	m	0.53	1.40	0.86	1.21	0.22	0.30	0.22	1.40	0.75
UF thickness	cm	4.5	2.0	3.0	2.0	0.75	2.0	1.5	4.5	2.5
Limnology										
DOC	mg L^{-1}	7.6	5.9	3.8	6.9	8.7	7.7	3.8	8.7	6.8
TSS	mg L^{-1}	6.3	2.8	3.7	2.5	24.3	22.2	2.5	24.3	10.3
DOC/TSS		1.2	2.1	1.0	2.8	0.4	0.3	0.3	2.8	1.3
TP	µg L^{-1}	39.7	36.3	25.9	24.7	74.7 [a]	67.5	24.7	74.7 [a]	44.8
Chl-a	µg L^{-1}	4.3	3.2	3.0	3.3	5.2	5.0	3.0	5.2	4.0
pH		6.6	6.3	6.3	6.3	7.2	6.2	6.2	7.2	6.5
Conductivity [a]	µS cm^{-1}	46	38	61	36	61	47	36	61	48
Top of oxycline [b]	m	1.0–1.5	1.5–2.0	2.0	1.5	0.5–1.5	0.5–1.0	0.5	2.0	1.2
Sampling/analyses										
Sediment trap depth	m	1.0	1.75	2.25	1.5	1.25	1.5	1.0	2.25	1.5
Type of sediment trap		passive	passive	passive	active	passive	active			
LOI measurements		x	x	x	x	x	x			
Geochemistry (ICP)			x	x		x				

UF, upper facies (i.e., top lacustrine sediments in retrieved cores); DOC, dissolved organic carbon; TSS, total suspended solids; TP, total phosphorus; Chl-a, chlorophyll-*a*; LOI, loss-on-ignition; ICP, inductively coupled plasma spectrometry.

Morphological properties were measured in July 2007 (Bouchard et al., 2011), and limnological properties were measured in July 2006 or otherwise specified (I. Laurion, unpublished data).

[a] 2009 data.

[b] Range of 2006, 2007 and 2009 data (oxygen profiles).

free conditions and covered a 25-km^2 area (center at 55°21.14′N, 77°32.37′W). The panchromatic band had a pixel size of 61 cm on the ground, thus comparable to the aerial photographs. The Quick-Bird image (Geotiff "ortho-ready" format, 16-bit) was geometrically corrected using the cubic convolution resampling method. It was then used to rectify and georeference the aerial photographs in ArcMap module (ArcGIS software version 10.0) using seven ground control points (GCP) evenly distributed on the ground (i.e., the four corners plus three GCP in the central part). This resulted in a total root mean square error (RMSE) of 4.28 pixels (1.8 m).

Five classes of areas were manually digitized for both periods (1959 vs. 2006) in a delimited area of ~ 0.25 km^2 (630 m × 400 m), including (1) permafrost mounds (palsas/lithalsas), (2) thermokarst ponds, (3) dense tree vegetation (>50% of the surface, mainly black spruce), (4) creek, and (5) remaining area (Figs. 2 and 3). Deciduous shrubs (e.g., *Salix*, *Betula*, *Alnus*) could not be separated from the surrounding landscape (e.g., herbaceous plants, mosses), thus they were included in the "remaining area." Manual delineation of land and water surfaces turned out to provide conclusive results with panchromatic high spatial resolution images, such as aerial photographs and QuickBird

imagery (Sannel and Brown, 2010; Sannel and Kuhry, 2011). Permafrost mounds, much more abundant in 1959, were easily recognized and delineated using the stereoscopic visualization of overlapping adjacent aerial photographs. Digitized polygons were converted into surfaces (m^2) and percentages of the delimited area for both periods. The distance (m) from the center of selected ponds in relation to the rocky hill outcrops to the west and the steeply embedded creek to the east was also digitized in order to characterize their spatial variability along the topographical and hydrological gradients.

SEDIMENT TRAPS, SOIL SAMPLING, AND LIMNOLOGY

To investigate sediment sources and pathways within thermokarst systems, we combined sediment trap, peripheral soil, and lacustrine sediment sampling. First, two sediment flux sensors equipped with an optical system (infrared light-emitting diodes and light-sensitive phototransistors) and a datalogger (one measurement every 6 hours) were installed in summer 2007 and retrieved in summer 2008 to record the precise timing and amount of sedimentation during the year (Appendix Fig. A2).
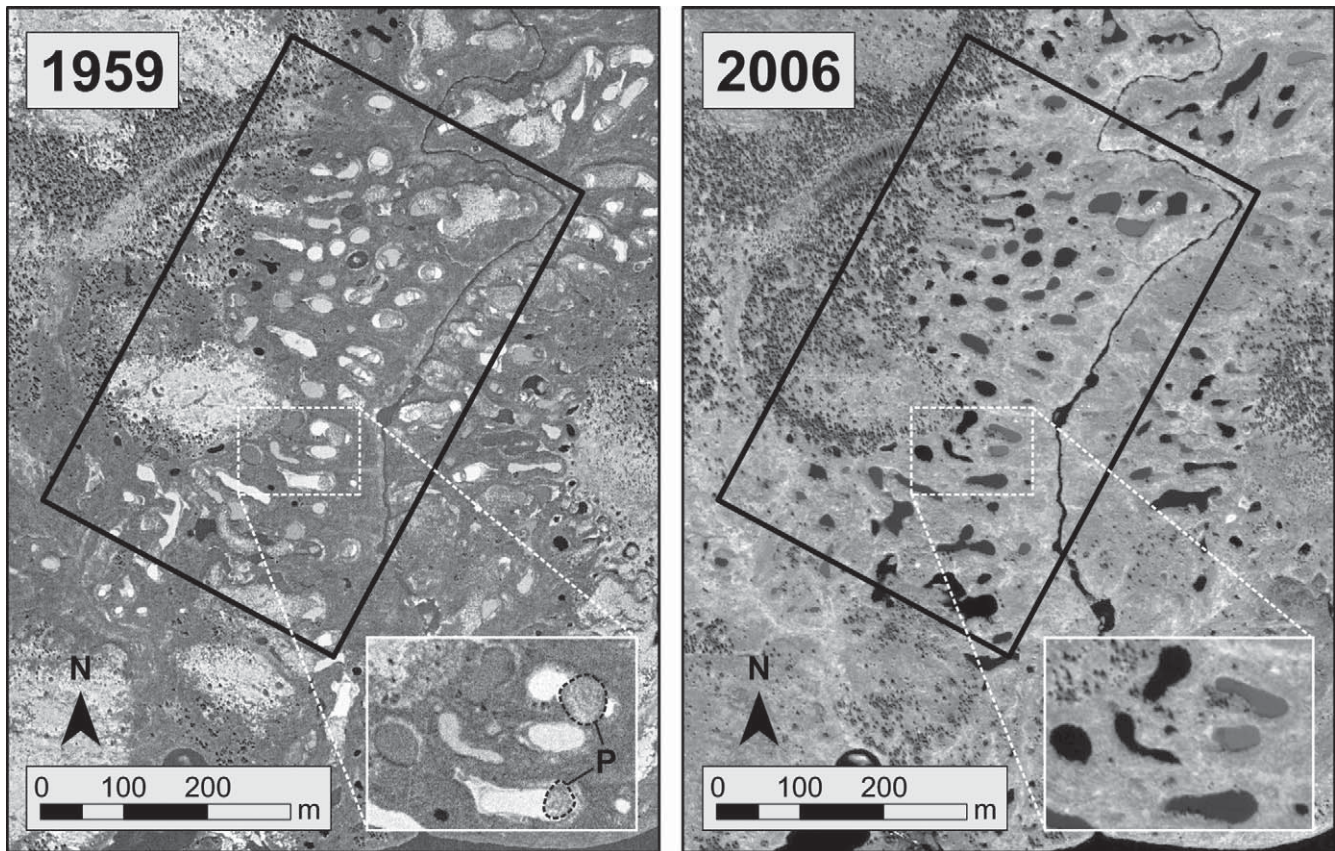
FIGURE 2. Black and white aerial photograph (left) and QuickBird panchromatic satellite image (right) used to perform spatio-temporal mapping (1959 vs. 2006). Several permafrost mounds were still visible in 1959 ("P" in bottom-right enlargement) and easily digitized using the stereoscopic visualization of overlapping adjacent aerial photographs. The oblique bold rectangle represents the delimited area of ~0.25 km² (630 m × 400 m) in which the mapping was done (results in Fig. 3).

These *active* sediment traps were designed to provide a continuous voltage output data—proportional to the number of light sensors progressively blocked as sediments accumulate in the vessel—which were then transformed back to sediment depths, thus accumulation rates (Lamoureux, 2005). They were deployed in two limnologically contrasting ponds: a humic-rich black-colored pond (K12) and a turbid beige-colored pond (K20) (Table 1). Due to generally low accumulation rates in high latitude aquatic systems (Wolfe et al., 2004), a 92-cm² funnel was mounted on top to provide a 16:1 amplification of incoming sediment. The sensors were attached to a mooring line, with the buoy submerged at a minimum water depth of 0.75–1 m to avoid being stuck in and/or displaced by the ice cover during the winter. The trap was fixed 25–50 cm below the buoy (i.e., 1–1.25 m above the weight or pond bottom). Second, *passive* sediment traps (consisting of a 50-mL plastic tube) collecting bulk sediment during a full annual cycle were also installed over the same period (Appendix Fig. A2) using a similar mooring line (but with a soda bottle with comparable dimensions acting as funnel) in the remaining ponds (Table 1). Sediment trap material was sealed in the field (in plastic bottles) and brought back to the laboratory, where it was kept in the dark at 4 °C.

Additional sediment samples were collected from the peripheral ridges of ponds in summer 2008 (Appendix Fig. A2). These samples were collected with a handheld auger at an ap-proximate depth of 30–50 cm. For each pond, two or three samples were taken and the resulting data were averaged. These sediments were transferred into polyethylene bags (Whirl-Pak®) and brought back to the laboratory (in the dark at 4 °C). Finally, to encompass the whole thermokarst system, we included in the present study results from surficial lacustrine sediments (the uppermost 0.5 cm) extracted from sediment cores analyzed for lithostratigraphic and biostratigraphic proxies and already presented in companion papers (Bouchard et al., 2011, 2013). Among these data, we present diatom-inferred DOC concentrations in surface sediments based on fossil diatom valves retrieved by standard techniques (for methodological details, see Bouchard et al., 2013.

All sediment samples (traps, peripheral ridges, and surficial lacustrine sediments) were transferred into glass bottles and dried at 105 °C for 24 hours. Loss-on-ignition (550 °C for ~4 h) was performed on subsamples of ~0.5 g, giving an approximation of organic matter content (Heiri et al., 2001). Finally, ~0.25 g of dried material from traps and surface sediments in three ponds was used to perform ICP-OES (inductively coupled plasma–optical emission spectrometry) and ICP-MS (inductively coupled plasma–mass spectrometry) measurements on major and minor or trace geochemical elements, respectively. Sediments were ground, homogenized, and completely digested with HNO_3, $HClO_4$ and HF. Acids were evaporated to near dryness and resi-

dues redissolved in a HNO$_3$ 2.7% solution (McLaren et al., 1995). Certified materials MESS-3 and PACS-2 from the National Research Council of Canada (NRCC) were used to determine precision and accuracy. Detailed results, as well as detection limit, precision, and accuracy for each detected element, are given in Appendix Tables A1 and A2.

Limnological data (e.g., DOC, TSS, and pH) were collected in summer 2006, 2007, and 2009 and partly reported by Laurion et al. (2010) for the year 2007. Some of these data were used in the present study to investigate the relationships between limnology, geomorphology, and sedimentology of thermokarst systems. If not otherwise specified, the 2006 data series was used because (1) there were fewer missing values for all sampled ponds during that year, and (2) they precede surficial sediment sampling (2007), so the limnological conditions likely had enough time to be "recorded" in surface sediments, allowing limnology-sedimentology comparisons. Remote sensing and geochemical results were compared to the limnological properties available from the six studied ponds (Table 1). Given the small sample size, we only report highly significant correlations with coefficients $r \geq 0.811$ to $r \geq 0.917$, which are the threshold values for $p < 0.05$ and $p < 0.01$, respectively (Sokal and Rohlf, 1995). Normality tests were performed on highly significant correlations and were found to be successful ($p \gg 0.05$).

Results

LANDSCAPE EVOLUTION (1959–2006) IN THE AREA

Surface areas occupied by permafrost mounds, thermokarst ponds, and dense tree vegetation have changed during the past 50 years, as shown in Figure 3 and Table 2 (upper section). The most drastic changes involved permafrost (96% decrease) and tree vegetation (327% increase), with no such significant change in thermokarst pond surface areas (2.5% decrease). In 1959, permafrost mounds represented nearly 9% of the landscape ($>22 \times 10^3$ m^2) and were mostly concentrated near the creek running along the eastern part of the study site. In 2006, only one mineral mound (lithalsa) was still present, although showing evidence of severe thawing and settlement (large turbid thermokarst ponds rapidly developing in the surroundings). In contrast, dense tree vegetation increased more than three times during the same period, evolving from a thinly scattered coverage (2.4% of the landscape, $<6 \times 10^3$ m^2), concentrated in the western part of the study site in 1959, to a notably more abundant coverage (>10% of the landscape, 25×10^3 m^2) and migrating toward the east (along the topographic-hydrologic gradient) in 2006. Finally, thermokarst pond surface areas showed no significant change between 1959 and 2006, representing ~9% of the landscape ($>22 \times 10^3$ m^2) for both periods. This proportion is two to three times higher than values estimated for

TABLE 2

Changes in permafrost mound, thermokarst pond, and vegetation surface areas (upper section), and in thermokarst pond characteristics (lower section) between 1959 and 2006.

|		Year		
		1959 (aerial photos)	2006 (satellite image)	Variation
Surface areas				
Permafrost mounds	m^2	22,350	820	−21,530
	%	8.9	0.3	−96.3
Thermokarst ponds	m^2	22,790	22,210	−580
	%	9.1	8.9	−2.5
Dense vegetation (> 50 %)	m^2	5940	25,370	+19,430
	%	2.4	10.2	+327.1
Remaining area	m^2	198,720	201,400	+2680
	%	79.6	80.6	+1.3
Total	m^2	249,800	249,800	–
Thermokarst pond characteristics				
Number of ponds	n	107	79	−28
	%			−26.2
Mean pond size	m^2	213.0	281.1	+68.1
	%			+32.0
Median pond size	m^2	142.4	213.9	+71.5
	%			+50.2
Minimum pond size	m^2	16.7	12.6	−4.2
	%			−24.8
Maximum pond size	m^2	922.4	2067.1	+1144.6
	%			+124.1
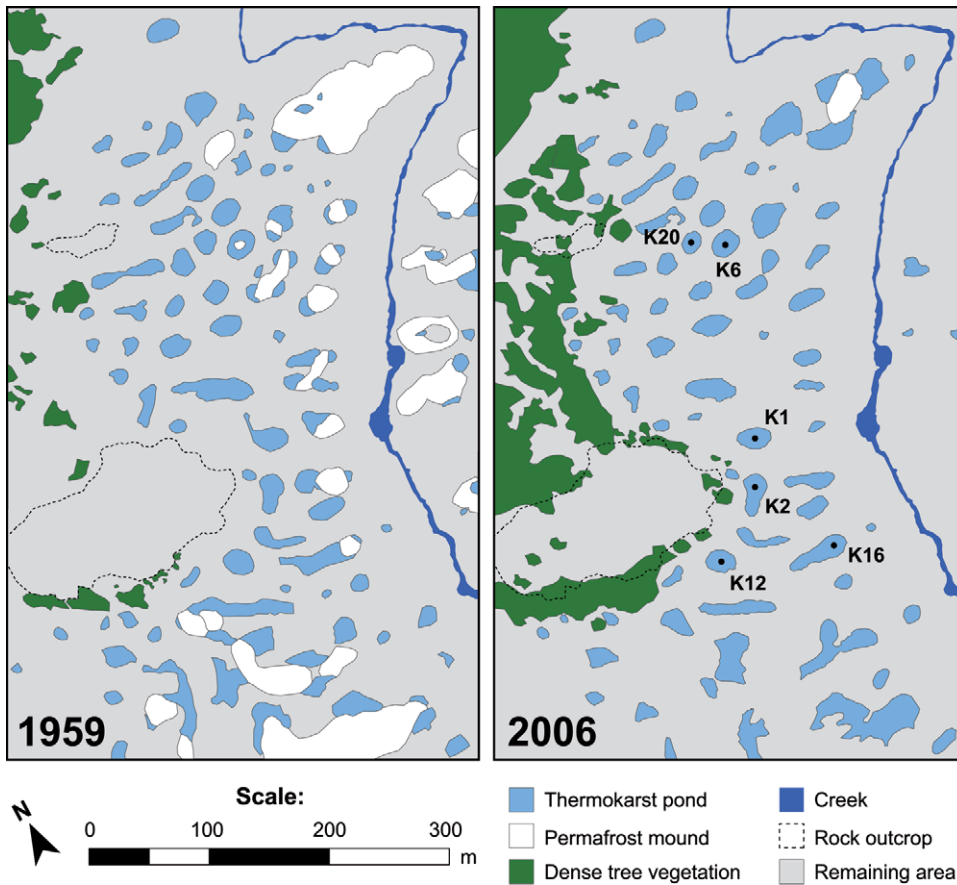
FIGURE 3. Thermokarst pond, permafrost mound, and vegetation surface areas in July 1959 and July 2006 (enlargement from the oblique rectangle of Fig. 2). Only one permafrost mound (also identified by the red circle in Fig. 1) is still visible in 2006. Rock outcrops to the west (dashed line) and a steeply embedded creek to the east (dark blue) are also shown. Sampled ponds (numbers as in the text) are identified on the 2006 map.

the whole northern hemisphere, although from much larger lakes (>0.1 km²; Smith et al., 2007).

Despite showing few changes in spatial coverage (total surface area), thermokarst pond numbers and individual sizes greatly evolved during the past five decades, as shown in Figure 4 and Table 2 (lower section). Between 1959 and 2006, pond numbers decreased from 107 to 79 (–26%), corresponding to generally larger ponds in recent years since total area changed little. Indeed, both mean and median pond sizes increased from 213 to 281 m² (+32%) and from 142 to 214 m² (+50%), respectively. While the minimum pond size slightly decreased from ~17 to 13 m² (–25%), the maximum pond size markedly increased from 922 to 2067 m² (+124%). This is further detailed when pond sizes are separated in 100 m² classes (Fig. 4): small-sized ponds (<200 m²) represented cumulatively more than 60% in 1959, but less than 50% in 2006. The smallest ponds (0–100 m²) showed the most important change in abundance between 1959 and 2006, with a >50% decrease (from 41 to 19). The observed increase in average pond size is partly caused by the merging of two or three ponds. During the same period, the relative proportion of medium-sized ponds (200–700 m²) has generally increased, although their individual size was slightly reduced (see below).

MODERN DYNAMICS IN SAMPLED PONDS

As mentioned above, thermokarst pond total surface areas have remained relatively constant in recent decades around the

study site, which resulted—with reduced pond numbers—in generally larger ponds (Table 2, Figs. 3 and 4). The individual surface areas of the six sampled ponds have shown relatively minor changes over the past 50 years (Table 3, upper section). One pond slightly increased in size by 4% (K6), another pond showed no significant change (K2), and the others have decreased by ~10% (K12, K16) or ~20% (K1, K20). Overall, among the sampled ponds the trend is inverse to the general one, with mean surface area slightly reduced by about 10%. Distances from each sampled pond to the outcropping rocky hill (west) or the steeply embedded creek (east) are also included in this section of Table 3, as they will further support proposed limnology-geomorphology-sedimentology relationships among ponds in the discussion. The six ponds sampled are generally located closer to the rocky hill (mean distance = 66 m) than to the creek (mean distance = 117 m).

Physical (loss-on-ignition, LOI) and geochemical (S, P, Fe, Mg, and Ti) measurements made *inside* (sediment traps), *underneath* (surface sediments), and *around* (peripheral ridges) thermokarst ponds showed contrasting results (Table 3, lower section). Mean LOI in sediment traps was around 32% but appeared highly variable, ranging from 10% in turbid beige pond K16 to 69% in humic black pond K2. LOI results were lower and less contrasting in surface sediments and peripheral ridges, with mean values of ~8% (6.5–10%) and ~5% (1.5–9%), respectively. Consequently, LOI ratios were far higher when trap data were involved (i.e., trap/sediment or trap/ridge ratios). Concentrations of selected geochemical elements are also presented for three contrasting ponds in the
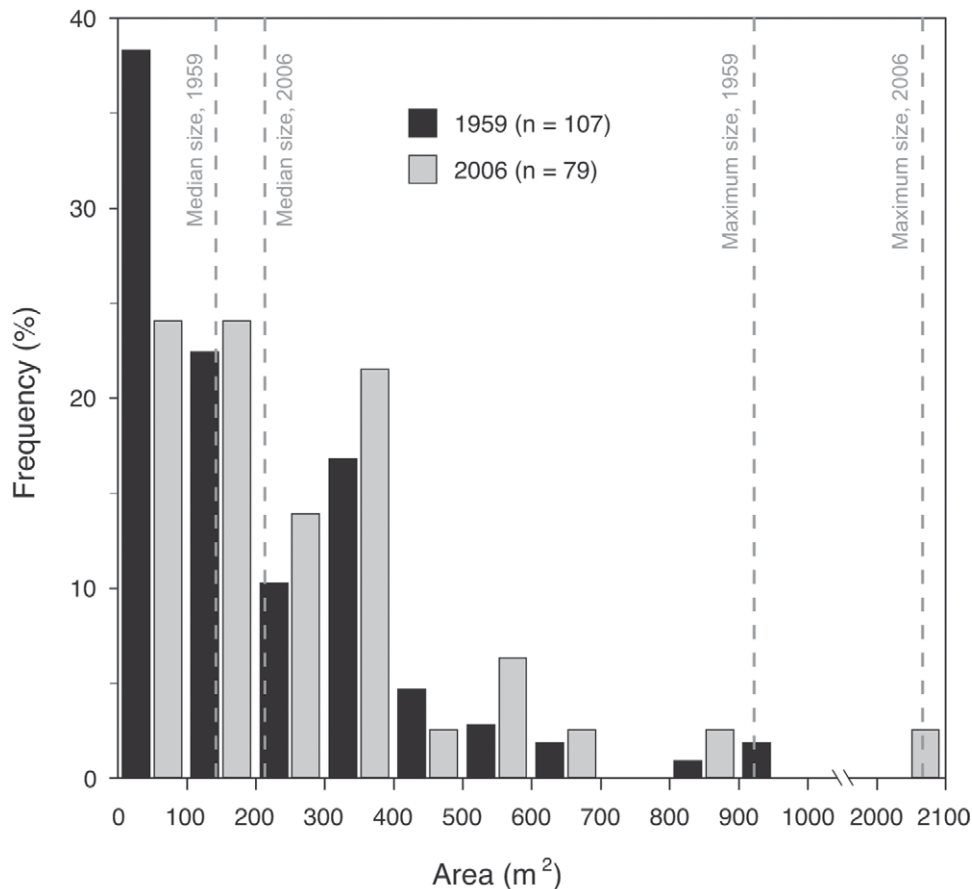
FIGURE 4. Relative frequencies of thermokarst ponds of various sizes (area in m²) in 1959 (black bars) and 2006 (gray bars). Median and maximum pond sizes are shown for both periods. Note the lack of ponds within the size range between 1000 and 2000 m².

lower section of Table 3, including elements showing affinity for organic matter and/or sensitive to redox conditions (S, P, and Fe) and mostly detrital or carbonate-derived elements (Ti and Mg). In pond K2, S-P-Fe concentrations were much higher in the trap than in surface sediments, resulting in high (trap/sediments) ratios of S (14.0), P (9.7), and Fe (2.0). Contrastingly, detrital and carbonate elements appeared ~50% less concentrated in the trap compared to surface sediments (Ti ratio = 0.5; Mg = 0.4). In pond K6, geochemical elements were slightly more concentrated in the trap (S ratio = 1.2; P = 4.2; Fe = 1.5) or showed similar concentrations (Ti ratio = 0.9; Mg = 1.0) compared to surface sediments. Finally, pond K16 results were comparable between trap and surface sediments, resulting in ratios of ~1 (except P = 1.5).

The two studied ponds in which *active* sediment traps (flux sensors) were installed showed strongly contrasting results (Fig. 5). In pond K12, the voltage output increased sharply twice during summer 2007 (early July and late July–early August), corresponding to episodes of rapid sedimentation in the trap, and coinciding with relatively high rainfalls in the region. In early September 2007, an unexpectedly low output was recorded, likely due to the entrapment of a large aquatic insect (Coleoptera, genus *Dytiscus*) that may have disturbed already settled sediments and subsequently biased measured fluxes of settling particles (Appendix Fig. A2). From that time, voltage outputs remained remarkably constant, except for two subtle peaks during snowfall episodes in mid-September 2007 and mid-May 2008 (thus

likely outside the ice-cover period). Pond K20 provided a very different trend. Voltage output increased slowly in summer 2007, slightly faster in early fall 2007 (September-October), and then gradually decreased to reach low values during winter 2008. The only exception was the remarkable voltage peak (i.e., very high accumulation rate) in early January 2008, associated with higher-than-average temperature (near 0 °C) and 3–4 days of snowfall recorded at the weather station. Finally, two last episodes of increasing voltage output occurred during the second half of May 2008 and in early July 2008, likely due to late-spring snowfall and early summer rainfall, respectively. It is worth noting that these ponds do not totally freeze in winter, as internal probes indicated temperatures between 4 °C and 12 °C (data not shown).

LIMNOLOGY, GEOMORPHOLOGY, AND SEDIMENTOLOGY RELATIONSHIPS

Spatio-temporal analysis (remote sensing) of the studied ponds and their surroundings, as well as the investigation of sediment sources and pathways within them, provided contrasting results depending on pond properties and morphology. Some of these correlations are presented in Figure 6, although complete data are provided as a correlation matrix in Appendix Table A3. First, the distance from the center of each pond to the rocky hill (to the west) was significantly correlated with water conductivity ($r^2 = 0.85$, $p < 0.01$) (Fig. 6, part a). This relationship may be re-

TABLE 3

Results from spatio-temporal mapping (upper section) and physical/geochemical analyses conducted inside (sediment traps), underneath (lacustrine sediments), and around (peripheral ridges) thermokarst ponds (lower section).

		K1	K2	K6	K12	K16	K20	Min	Max	Mean
		brown	black	blue-green	black	beige	beige			
Mapping results										
1959 surface area	m²	494.3	469.5	369.1	416.9	694.2	277.6	277.6	694.2	453.6
2006 surface area	m²	389.0	470.4	384.5	364.9	635.6	221.4	221.4	635.6	411.0
Variation (1959–2006)	m²	−105.3	+0.9	+15.4	−52.0	−86.0	−56.1	−105.3	+15.4	−47.2
	%	−21.3	+0.2	+4.2	−12.5	−11.9	−20.2	−21.3	+4.2	−10.3
Distance from hill	m	30.1	34.2	125.5	32.4	103.8	71.6	30.1	125.5	66.3
Distance from creek	m	77.9	90.4	141.8	152.0	63.3	174.9	63.3	174.9	116.7
Physical and geochemical results										
LOI, trap	%	39.3	69.3	15.6	41.9	10.2	12.3	10.2	69.3	31.5
LOI, sediments	%	6.5	10.1	8.2	9.3	8.0	7.0	6.5	10.1	8.2
LOI, ridge	%	4.9	8.9	1.5	3.7	4.3	8.0	1.5	8.9	5.2
LOI ratio, trap/sediments		6.1	6.8	1.9	4.5	1.3	1.8	1.3	6.8	3.7
LOI ratio, trap/ridge		8.0	7.8	10.5	11.4	2.4	1.6	1.6	11.4	6.9
LOI ratio, sediments/ridge		1.3	1.1	5.5	2.5	1.9	0.9	0.9	5.5	2.2
S, trap	µmol g⁻¹		190.2	52.9		16.0		16.0	190.2	86.4
S, sediments	µmol g⁻¹		13.6	43.2		14.8		13.6	43.2	23.8
S ratio, trap/sediments			14.0	1.2		1.1		1.1	14.0	5.4
P, trap	µmol g⁻¹		311.4	114.1		47.4		47.4	311.4	157.6
P, sediments	µmol g⁻¹		32.0	27.3		32.0		27.3	32.0	30.4
P ratio, trap/sediments			9.7	4.2		1.5		1.5	9.7	5.1
Fe, trap	µmol g⁻¹		1479.4	1034.5		809.7		809.7	1479.4	1107.8
Fe, sediments	µmol g⁻¹		755.5	694.4		795.4		694.4	795.4	748.4
Fe ratio, trap/sediments			2.0	1.5		1.0		1.0	2.0	1.5
Mg, trap	µmol g⁻¹		321.2	588.9		675.7		321.2	675.7	528.6
Mg, sediments	µmol g⁻¹		727.8	609.6		749.0		609.6	749.0	695.5
Mg ratio, trap/sediments			0.4	1.0		0.9		0.4	1.0	0.8
Ti, trap	µmol g⁻¹		30.9	56.3		68.9		30.9	68.9	52.0
Ti, sediments	µmol g⁻¹		67.9	61.5		68.0		61.5	68.0	65.8
Ti ratio, trap/sediments			0.5	0.9		1.0		0.5	1.0	0.8

lated to the pond position along the topographical and hydrological gradients: ponds farther to the east overlying thicker postglacial marine sediments were slightly more alkaline and saline. In contrast, ponds closer to the hill were underlain by thinner marine sediment deposits and had more dilute, less conductive waters. Distance from the hill was also inversely correlated ($r^2 = 0.71$, $p < 0.05$) with the LOI contrast between sediment traps and surface sediments (Appendix Table A3). This confirms that ponds closer to the rocky hill (and closer to dense vegetation; see Fig. 3) had higher organic matter contents in the water column compared to surface sediments, as opposed to ponds located farther east with more turbid (less organic) waters.

Second, diatom-inferred DOC (DI-DOC) in surface sediments, modeled and presented by Bouchard et al. (2013) for these ponds, was inversely correlated ($r^2 = 0.91$, $p < 0.01$) to LOI contrast between surface sediment and peripheral ridges (Fig. 6, part b). DI-DOC results obtained from surface sediments can be considered reliable given their significant correlation with measured DOC ($r^2 = 0.77$, $p < 0.02$) in the water column (Appendix Table A3). Pond K6 stood clearly apart from other ponds, due to very low LOI in its peripheral ridge (<1.5%) as compared to the mean value for all sampled ponds (5.2%). This blue-green pond had by far the lowest DOC values among all sampled ponds (Table 1).
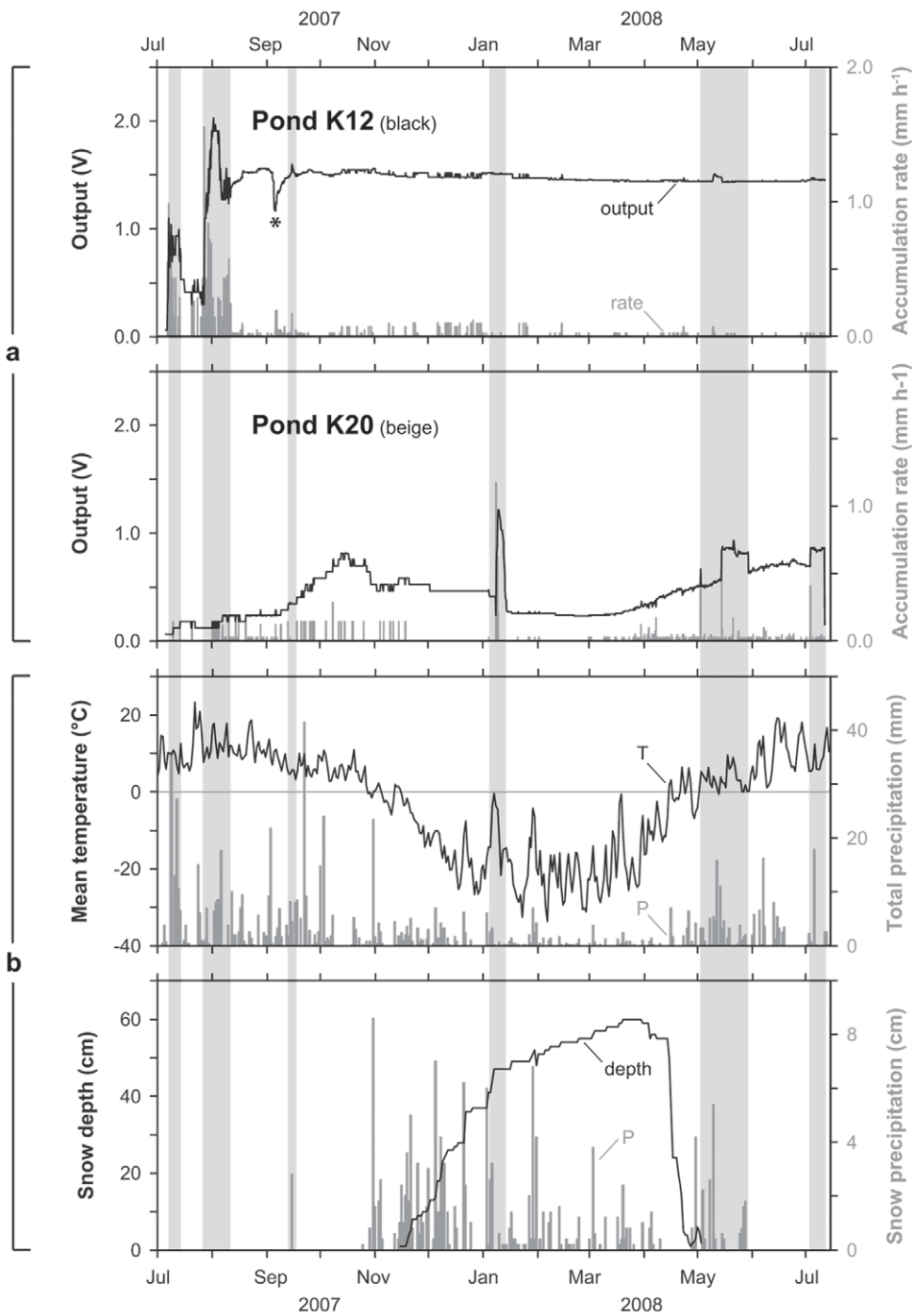
FIGURE 5. Active (flux sensor) sediment trap and meteorological data from 06 July 2007 to 11 July 2008. (a) Voltage outputs (black curves), proportional to accumulated sediments, and sediment accumulation rates (gray bars) in two limnologically contrasting ponds, the humic/black-colored pond K12 (upper graph) and the turbid/beige-colored pond K20 (lower graph). An unexpectedly low output (*) in early September 2007 is likely due to a large aquatic insect that may have disturbed already settled sediments in pond K12 (Appendix Fig. A2). Data recorded at 6-h time steps by sediment flux sensors (Lamoureux, 2005). (b) Mean temperature (black curve, upper graph), total precipitation (gray bars, upper graph), snow depth (black curve, lower graph) and snow precipitation (gray bars, lower graph) at the Kuujjuarapik-Whapmagoostui weather station. Daily data retrieved online (Environment Canada, 2012b). Vertical gray-shaded areas indicate enhanced sedimentation episodes (recorded either in K12 or K20) likely related to meteorological events, such as heavy rainfall/snowfall or winter temperatures near 0 °C.

Discussion

POND MORPHO-LIMNOLOGY AS A CONTROLLING FACTOR ON SEDIMENTOLOGY

As mentioned above, we found a significant, inverse relationship between DI-DOC and LOI ratio (sediment/ridge) (Fig. 6, part b). In other words, the more organic-rich the peripheral ridges are (i.e., low sediment/ridge ratio), the more abundant high-DOC diatom species (e.g., genera *Frustulia*, *Caloneis*, *Pinnularia*) will be. This confirms the important control of highly organic surround-

ings or semi-dry aerophilous, bryophilous substrates (e.g., peat and moss patches on peripheral ridges at the initial pond inception) on diatom community composition, as observed at this particular site and elsewhere in tundra wetlands of the Canadian Arctic (Ellis et al., 2008). Moreover, DI-DOC in these ponds has slightly decreased in recent years, which has been attributed by Bouchard et al. (2013) to (1) the variable impact of peat patches in pond catchments during their initial development, (2) their apparently small catchments, and (3) the influence of abundant mineral (organic-poor) particles eroded from their littoral zones, settling, and ad-
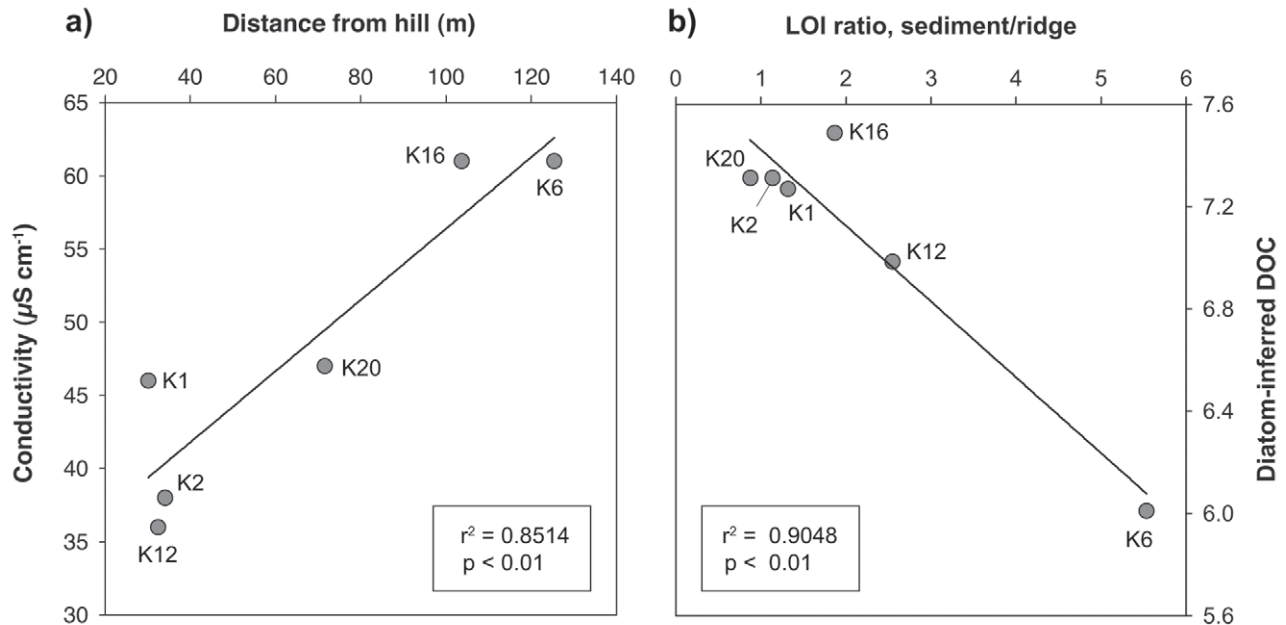
FIGURE 6. Correlation plots between selected limnological properties, landscape mapping, and biogeochemical results measured inside (sediment traps), underneath (lacustrine sediments), and around (peripheral ridges) thermokarst ponds (n = 6). More correlations are presented in Appendix Table A3. See Bouchard et al. (2013) for details on the determination of diatom-inferred DOC.

sorbing dissolved organic molecules, thus progressively isolating the initial DOC source from the water column. This evolutional sequence may contribute to the continuous "transfer" of DOC from peripheral ridges—at least the organic-rich ones—to bottom sediments, associated with decreasing DOC in the water column. As a consequence, thermokarst pond evolution stages—their geomorphology—likely control their limnological and sedimentological properties, underscoring the major influence of autogenic (in situ) processes (e.g., vegetation and soil development, peat accumulation and erosion) in addition to allogenic forcing mechanisms (e.g., climate, geochemical leaching in the surroundings) on diatom community changes in the recent past.

Furthermore, sediment trap data provide evidence of direct links that exist between pond morphology (depth), limnology (oxycline position, redox conditions, organic matter, TSS), and sedimentology (dissolution vs. precipitation and transport of particles or chemical elements). Voltage outputs (proportional to accumulated sediments) and accumulation rates in active sediment traps (flux sensors) during a full annual cycle (Fig. 5) can be interpreted in relation to sediment trap position and the development of steep thermal/oxygenic stratification. In pond K12, the sensor was deployed at ~1.5 m depth, which corresponds to the top of the seasonal oxycline for this pond (Table 1). The sensor was thus located at a depth where it could detect autochthonous or detrital particle inputs resulting from enhanced productivity or surface runoff around the pond during the ice-free period. Such events likely occurred during relatively high temperature and heavy rainfall episodes in summer 2007. During the winter, voltage outputs remained remarkably constant, likely due to the ice cover build-up and its associated reduction in planktonic production and littoral erosion, but also because of partial obstruction of the sedimentation vessel by the large aquatic insect mentioned above (see Results section). The sensor deployed in highly turbid and

steeply stratified pond K20 was substantially below the top of the seasonal oxycline (1.5 m vs. 0.5–1.0 m, respectively), thus located in strongly oxygen-depleted waters for most of the year. The shaded and anoxic environment of this pond may have prevented high sedimentation rates (especially particulate organic matter), as indicated by generally lower voltage outputs compared to pond K12 (Fig. 5), even though this pond has more suspended solids than K12 (mainly inorganic particles like clays and silts, which have very low settling rates). In this regard, the gradually increasing voltage output in September–October 2007 may be related to fall overturn, occurring around this time of the year in the similar nearby pond K16 (Laurion et al., 2010). Nevertheless, the only exception to such relatively weak accumulation is the sharp sedimentation peak recorded in early January 2008, associated with higher-than-average temperature (near 0 °C). The resulting partial thawing of snow/ice in the surroundings possibly induced enhanced detritic inputs in this particular pond, although continuous snow depths and ice cover thickness measurements are not available for the study site to confirm this assertion. Under these circumstances, it is also difficult to explain why this specific regional meteorological warming event was not recorded in the other pond (K12), unless ice cover and snow depth were substantially different above and around it. Finally, these ponds do not totally freeze in winter, which is consistent with surface and bottom water temperatures recorded by Laurion et al. (2010) in nearby pond K16 during the same period, which revealed that both surface and bottom temperatures always remained above zero in winter, likely due to high snow entrapment over the ponds.

Sedimentological processes occurring in thermokarst ponds and their anaerobic sediments can have a significant influence on the carbon cycle in such systems, as methane production can be fueled by early diagenetic mechanisms occurring under anoxic conditions, such as sulfate reduction and acetate fermentation (Berner,

1980; Walter et al., 2008). Investigating thermokarst lake sediments in a partly thawed palsa peatland of western Siberia, Audry et al. (2011) observed intense microbial mineralization of organic matter (mainly derived from peat lixiviation) in surface sediment pore water under anoxic conditions. They also documented a shift in mineralization pathways during the course of lake development and maturation (from small shallow ponds to partly drained larger lakes), from nitrate and sulfate reduction in small ponds to reductive dissolution of Fe and Mn oxyhydroxides in larger drained lakes. These results obtained in surficial anaerobic sediments greatly differ from the observations made in the overlying water column of the same thermokarst lakes, where aerobic respiration of heterotrophic bacterioplankton releases CO_2 to the atmosphere through DOC consumption (Shirokova et al., 2009; Pokrovsky et al., 2011). This marked difference could also be partly related to contrasting water balances and pond/lake water sources (thawed permafrost ice vs. precipitation-evapotranspiration), as reported from eastern Siberia (Abnizova et al., 2012). In spite of shallow water depths, thermokarst ponds at our study site are seasonally strongly stratified through most of the year and are net sources of methane, with large increases observed near the surface sediments in the anoxic/hypoxic hypolimnion (Laurion et al., 2010). This steep thermal stratification is a direct consequence of the high humic content and especially the very high turbidity in most of these systems, which is in turn related to sedimentation dynamics. This underscores the major influence of bottom water limnology and sedimentology on biogeochemical processes in thermokarst systems, as already suggested for our study site.

THERMOKARST LANDSCAPE EVOLUTION: SPATIAL AND TEMPORAL CONSIDERATIONS

The spatio-temporal mapping of the main landscape features over the past 50 years, as well as the investigation of modern sediment sources and pathways in thermokarst ponds, have documented three mechanisms: (1) permafrost mound thawing, modifying the local hydrology and geomorphology and providing new inputs of sediments, water, and chemical elements; (2) thermokarst pond inception and evolution, acting as temporary biogeochemical reservoirs and potentially contributing to local GHG emissions from strongly stratified waters to the atmosphere; and (3) vegetation development and densification, driving changes in snow depth distribution, thus affecting soil properties (e.g., heat, humidity).

Results from the spatio-temporal mapping indicated that the near disappearance of permafrost-affected areas was accompanied by a remarkable increase in vegetation cover (Table 2, Figs. 3 and 4). In 1959, permafrost mounds were mostly concentrated near the creek in the east, thus topographically (and hydrologically) lower than already formed thermokarst ponds in the west (Fig. 3). Given their closer location to the center of this postglacial valley, these mounds were likely underlain by thicker frost-susceptible marine sediments, potentially containing ice layers that would contribute to delay their complete thawing and subsidence by the latent heat effect. Such frost-susceptible marine deposits (several meters thick), containing up to 80% of ice in the form of centimeter-scale segregated ice lenses and therefore delaying final thermokarst subsidence of the overlying surface layers, were indeed described along the southeastern coast of Hudson Bay (Allard et al., 1996). However, more detailed cryostratigraphic or geophysical work (e.g., thermistor cables, boreholes, and ground-penetrating radar) is needed to further assess the impact of this mechanism at our study site.

In 1959, already mature thermokarst ponds were mostly located in the western part of the study area, near the outcropping rocky hills (Fig. 3). These were thus more likely to be influenced by surface and groundwater flows originating from nearby hills and slopes. Such sheltered hillslopes generally accumulate more snow, which contributes to the general water and heat flows in the area. Combined with the lack of thick ice-rich marine deposits, the western part of the study area likely became an early source of thermal flux by surface and groundwater flows. Permafrost thawing and subsidence and related thermokarst development, caused by lateral heat flow along hydrological gradients, have been observed and reported by Calmels et al. (2008a, 2008b) from a rapidly degrading permafrost landscape in eastern Hudson Bay. Again, detailed geophysical data are not available at our study site, although such processes likely occurred in comparable permafrost landscapes.

Vegetation changes between 1959 and 2006 also appeared to follow the local topography, hydrology, and geomorphology. In 1959, tree-covered areas were rather sparse and mostly located in the western part of the study site (Figs. 2 and 3), thus at slightly higher elevation along the local topographical-hydrological gradient, but also on relatively thin surficial postglacial marine deposits. In 2006, tree vegetation was still more abundant in the western area but also had succeeded in migrating eastward, even partly surrounding several thermokarst ponds. Shrub development and expansion was possibly following the same pattern, as observed elsewhere in subarctic Québec (Ropars and Boudreau, 2012; Tremblay et al., 2012). Thus, over the last ~5 decades, vegetation, permafrost, and thermokarst dynamics proceeded from the west (thin frost-susceptible surface deposits, higher topography, upstream location) to the east (thicker deposits, lower topography, downstream location). The typical low-lying fen or bog vegetation surrounding several ponds (e.g., sedges, mosses, dwarf willows) was not distinctly mapped at our study site because of difficult land-water separation of such surfaces on black-and-white images (Sannel and Brown, 2010). However, the monitoring over the past 50 years of a subarctic permafrost peatland containing many thermokarst ponds (Payette et al., 2004) revealed that rapid permafrost thawing caused by recent climate change has resulted in two concurrent trajectories linked to the carbon budget: (1) thermokarst pond inception and mature development (assumed as carbon source), and (2) rapid terrestrialization by fen/bog vegetation growth and peat accumulation (assumed as carbon sink). These contrasting natural mechanisms were possibly also acting at our study site, although active terrestrialization was not clearly visible and may not be as efficient in turbid thermokarst ponds that are surrounded and underlain by impermeable silts and clays.

The studied thermokarst landscape is similar to many others formed during the Holocene along the eastern coast of Hudson Bay (Payette et al., 2004; Vallée and Payette, 2007; Calmels et al., 2008a), and also elsewhere in subarctic regions where permafrost is rapidly degrading since the early 20th century (e.g., Zuidhoff and Kolstrup, 2000; Sannel and Kuhry, 2011). However, most studies in these regions (including northeastern Canada) have considered thermokarst ponds as the final or transitional stage in the degradation sequence of permafrost mounds, or as an indicator of ancient periglacial forms (e.g., Allard et al., 1996; Matthews et al., 1997; Luoto and Seppälä, 2003; Payette et al., 2004; Calmels et al., 2008a). With the exception of recent work done in a subarctic palsa peatland of western Siberia (Shirokova et al., 2009; Audry et al., 2011; Pokrovsky et al., 2011), few studies have investigated the links between external (landscape) and internal (sedimentology, biogeochemistry) processes controlling thermokarst pond

evolution. Yet, sediments retrieved from these aquatic systems can provide useful information about their life cycle and responses to external climate and environmental changes.

The developmental stage of subarctic thermokarst ponds has been suggested as one of the major factors affecting their limnological properties (Breton et al., 2009), as it is likely to control their trophic state and stability (e.g., through microbial community composition, aquatic plant colonization, and reduced erosion/suspension of silts and clays). The temporal dynamics of thermokarst ponds and the duration of successional aquatic states should therefore have significant impacts on local biogeochemical fluxes. Mapping a series of thermokarst ponds (1959 vs. 2006) has shown that ponds formed before 1959 (e.g., K2, K12) were generally located near the outcropping rocky hill on the western side of the study area, whereas ponds formed more recently (e.g., K16) were closer to the creek on the eastern side (Fig. 3). These younger ponds ("post-1959") generally have very turbid waters (Fig. 1), although this relationship may not be as straightforward for other ponds because of the notable landscape heterogeneity in peat patches during early stages of pond formation (Pissart, 2002; Calmels et al., 2008a), possibly dependent on local topography (e.g., the position relative to the rocky hill) and the direction of dominant winds. Organic-rich peat layers were indeed found below lacustrine sediments in most of the study ponds Bouchard et al., 2013. Therefore, only the broad evolutionary stages of thermokarst ponds can be associated with some of their limnological characteristics (such as TSS content): the youngest ponds are all notably turbid and have thus a characteristic milky color. If a peat cover was still present when the corresponding permafrost mound thawed, it could have resulted in high DOC concentrations from peat lixiviation. Pond K16 is an example of such a young pond with high turbidity (TSS > 20 mg L^{-1}) and relatively high DOC (8.7 mg L^{-1}, clearly above the 6.8 mg L^{-1} mean for all sampled ponds; Table 1), in which a peat layer was observed below thin (<1 cm) lacustrine sediments (Appendix Fig. A3). In contrast, pond K6 has lower DOC and much lower TSS, and it lacked such a well-defined peat layer in retrieved cores, although some organic debris was found below the lacustrine sediments. (For detailed macro-/microscopic descriptions see Bouchard et al., 2011.) Therefore, a straightforward age-limnology relationship cannot be easily inferred from this kind of environment and is likely biased by the landscape-scale heterogeneity of peat deposits during pond inception. A more detailed peat sampling survey conducted around and underneath these ponds should provide new insights in this regard.

Recent landscape changes and related sedimentological processes are of great interest for understanding carbon-climate feedbacks, since GHG emissions at high latitudes may be determined by local factors such as topography, hydrology, and vegetation cover (e.g., Liblik et al., 1997; Christensen et al., 2004; Wickland et al., 2006; Flessa et al., 2008; Bäckstrand et al., 2010). With their highly organic waters and catchments, thermokarst ponds and lakes are expected to play a major role in future climate dynamics, either as a carbon source through GHG emissions (Walter et al., 2006; Schuur et al., 2008; Laurion et al., 2010), or as a carbon sink by accumulating peat through natural terrestrialization (Payette et al., 2004). However, the controlling processes involved have yet to be fully understood and quantified at different temporal and spatial scales. In this regard, studies such as the one presented here are a starting point, though more detailed hydro-ecological investigations (e.g., water and sediment stable isotope tracers like ^{18}O and thorough analysis of peat deposits) should help identify and interpret the biogeochemical processes involved.

Conclusions

Combining spatio-temporal mapping and sediment trap data, this study yielded new insights into climate-induced subarctic permafrost thawing and thermokarst pond dynamics over the last ~5 decades. As expected at this latitude, permafrost mound surface areas substantially decreased and palsas/lithalsas almost disappeared between the late 1950s and late 2000s. However, this change was not compensated by a corresponding increase in the total surface area occupied by thermokarst ponds, but rather by a remarkable threefold increase in vegetation cover. Moreover, the observed geomorphological and ecological changes (permafrost-thermokarst-vegetation) proceeded along the local topographical-hydrological gradient (from west to east), thus from "thin and ice-poor" to "thick and ice-rich" postglacial surface deposits, which likely delayed final surface subsidence in the eastern part of the study area. As a consequence, eastern thermokarst ponds are now generally younger (<50 years old) with more turbid and electrolyte-rich waters, compared to older (>50 years old) and more diluted and humic ponds in the west.

This study also shed light on sedimentological and geochemical processes occurring in strongly stratified thermokarst ponds with seasonal hypoxic/anoxic bottom waters. We demonstrated that the concentration of organic matter and chemical elements varied greatly—by an order of magnitude—among ponds and within the water column, and provided an integrated model of thermokarst pond geochemistry that combines aspects of pond morphology, limnology, and sedimentology. These findings confirm and refine recent paleolimnological reconstructions based on sediment core analyses from the same ponds, and underscore the importance of local landscape properties (e.g., geomorphology) that modulate regional forcing mechanisms (e.g., climate). Additional studies conducted in comparable thermokarst landscapes should provide more insights into large-scale landscape changes and their impacts on pond and lake sedimentological and limnological properties.

Acknowledgments

References Cited

Abnizova, A., Siemens, J., Langer, M., and Boike, J., 2012: Small ponds with major impact: the relevance of ponds and lakes in permafrost landscapes to carbon dioxide emissions. *Global Biogeochemical Cycles,* 26: GB2041, doi: http://dx.doi.org/10.1029/2011GB004237.

Agafonov, L., Strunk, H., and Nuber, T., 2004: Thermokarst dynamics in Western Siberia: insights from dendrochronological research. *Palaeogeography, Palaeoclimatology, Palaeoecology,* 209: 183–196.

Allard, M., and Seguin, M. K., 1987: Le pergélisol au Québec nordique: bilan et perspectives. *Géographie physique et Quaternaire,* 41: 141–152.

Allard, M., and Tremblay, G., 1983: La dynamique littorale des îles Manitounuk durant l'Holocène. *Zeitschrift für Geomorphologie, Supplementbände,* 47: 61–95.

Allard, M., Caron, S., and Bégin, Y., 1996: Climatic and ecological controls on ice segregation and thermokarst: the case history of a permafrost plateau in northern Quebec. *Permafrost and Periglacial Processes,* 7: 207–227.

Arlen-Pouliot, Y., and Bhiry, N., 2005: Palaeoecology of a palsa and a filled thermokarst pond in a permafrost peatland, subarctic Quebec, Canada. *The Holocene,* 15: 408–419.

Audry, S., Pokrovsky, O., Shirokova, L., Kirpotin, S., and Dupré, B., 2011: Organic matter mineralization and trace element post-depositional redistribution in Western Siberia thermokarst lake sediments. *Biogeosciences,* 8: 3341–3358.

Bäckstrand, P., Crill, P., Jackowicz-Korczyñski, M., Mastepanov, M., Christensen, T. R., and Bastviken, D., 2010: Annual carbon gas budget for a subarctic peatland, northern Sweden. *Biogeosciences,* 7: 95–108.

Barber, D. C., Dyke, A. S., Hillaire-Marcel, C., Jennings, A. E., Andrews, J. T., Kerwin, M. W., Bilodeau, G., McNeely, R., Southon, J., Morehead, M. D., and Gagnon, J.-M., 1999: Forcing of the cold event of 8,200 years ago by catastrophic drainage of Laurentide lakes. *Nature,* 400: 344–348.

Beilman, D. W., Vitt, D. H., and Halsey, L. A., 2001: Localized permafrost peatlands in Western Canada: definition, distributions, and degradation. *Arctic, Antarctic, and Alpine Research,* 33: 70–77.

Berner, R. A., 1980: *Early Diagenesis: a Theoretical Approach.* New York: Princeton University Press, 241 pp.

Bhiry, N., and Robert, E. C., 2006: Reconstruction of changes in vegetation and trophic conditions of a palsa in a permafrost peatland, subarctic Québec, Canada. *Ecoscience,* 13: 56–65.

Bouchard, F., Francus, P., Pienitz, R., and Laurion, I., 2011: Sedimentology and geochemistry of thermokarst ponds in discontinuous permafrost, subarctic Quebec, Canada. *Journal of Geophysical Research–Biogeosciences,* 116: G00M04, doi: http://dx.doi.org/10.1029/2011JG001675.

Bouchard, F., Pienitz, R., Ortiz, J. D., Francus, P., and Laurion, I., 2013: Palaeolimnological conditions inferred from fossil diatom assemblages and derivative spectral properties of sediments in thermokarst ponds of subarctic Quebec, Canada. *Boreas,* 42: 575–595, http://onlinelibrary.wiley.com/doi/10.1111/bor.12000/full.

Breton, J., Vallières, C., and Laurion, I., 2009: Limnological properties of permafrost thaw ponds in northeastern Canada. *Canadian Journal of Fisheries and Aquatic Sciences,* 66: 1635–1648.

Brosius, L. S., Walter Anthony, K. M., Grosse, G., Chanton, J. P., Farquharson, L. M., Overduin, P. P., and Meyer, H., 2012: Using the deuterium isotope composition of permafrost meltwater to constrain thermokarst lake contributions to atmospheric CH_4 during the last deglaciation. *Journal of Geophysical Research–Biogeosciences,* 117: G01022, doi: http://dx.doi.org/10.1029/2011JG001810.

Brown, J., Ferrians, O. J., Heginbottom, J. A., and Melnikov, E. S., 1998: Circum-Arctic map of permafrost and ground-ice conditions. Boulder, Colorado: National Snow and Ice Data Center/World Data Center for Glaciology.

Calmels, F., Allard, M., and Delisle, G., 2008a: Development and decay of a lithalsa in northern Quebec: a geomorphological history. *Geomorphology,* 97: 287–299.

Calmels, F., Delisle, G., and Allard, M., 2008b: Internal structure and the thermal and hydrological regime of a typical lithalsa: significance for permafrost growth and decay. *Canadian Journal of Earth Sciences,* 45: 31–43.

Carroll, M. L., Townshend, J. R. G., DiMiceli, C. M., Loboda, T., and Sohlberg, R. A., 2011: Shrinking lakes of the Arctic: Spatial relationships and trajectory of change. *Geophysical Research Letters,* 38: L20406, doi: http://dx.doi.org/10.1029/2011GL049427.

Christensen, T. R., Johansson, T., Ökerman, H. J., Mastepanov, M., Malmer, N., Friborg, T., Crill, P., and Svensson, B. H., 2004: Thawing sub-arctic permafrost: effects on vegetation and methane emissions. *Geophysical Research Letters,* 31: L04501, doi: http://dx.doi.org/10.1029/2003GL018680.

Dyke, A. S., and Prest, V. K., 1987: Late Wisconsinan and Holocene history of the Laurentide Ice Sheet. *Géographie physique et Quaternaire,* 41: 237–263.

Ellis, C. J., Rochefort, L., Gauthier, G., and Pienitz, R., 2008: Paleoecological evidence for transitions between contrasting landforms in a polygon-patterned High Arctic wetland. *Arctic, Antarctic, and Alpine Research,* 40: 624–637.

Environment Canada, 2012a: Canadian Climate Normals or Averages 1971–2000, http://climate.weatheroffice.gc.ca/climate_normals/index_e.html.

Environment Canada, 2012b: Climate Data Online, http://climate.weatheroffice.gc.ca/climateData/canada_e.html.

Flessa, H., Rodionov, A., Guggenberger, G., Fuchs, H., Magdon, P., Shibistova, O., Zrazhevskaya, G., Mikheyeva, N., Kasansky, O. A., and Blodau, C., 2008: Landscape controls of CH_4 fluxes in a catchment of the forest tundra ecotone in northern Siberia. *Global Change Biology,* 14: 2040–2056.

Heiri, O., Lotter, A. F., and Lemcke, G., 2001: Loss on ignition as a method for estimating organic and carbonate content in sediments: reproducibility and comparability of results. *Journal of Paleolimnology,* 25: 101–110.

Hillaire-Marcel, C., 1976: La déglaciation et le relèvement isostatique sur la côte est de la baie d'Hudson. *Cahiers de géographie du Québec,* 20: 185–220.

Hillaire-Marcel, C., Occhietti, S., and Vincent, J.-S., 1981: Sakami moraine, Quebec: a 500-km-long moraine without climatic control. *Geology,* 9: 210–214.

Jones, B. M., Grosse, G., Arp, C. D., Jones, M. C., Anthony, K. M. W., and Romanovsky, V. E., 2011: Modern thermokarst lake dynamics in the continuous permafrost zone, northern Seward Peninsula, Alaska. *Journal of Geophysical Research–Biogeosciences,* 116: doi: http://dx.doi.org/10.1029/2011JG001666.

Jorgenson, M. T., Shur, Y. L., and Pullman, E. R., 2006: Abrupt increase in permafrost degradation in Arctic Alaska. *Geophysical Research Letters,* 33: L02503, doi: http://dx.doi.org/10.1029/2005GL024960.

Kortelainen, P., Rantakari, M., Huttunen, J. T., Mattsson, T., Alm, J., Juutinen, S., Larmola, T., Silvola, J., and Martikainen, P. J., 2006: Sediment respiration and lake trophic state are important predictors of large CO_2 evasion from small boreal lakes. *Global Change Biology,* 12: 1554–1567.

Labrecque, S., Lacelle, D., Duguay, C. R., Lauriol, B., and Hawkings, J., 2009: Contemporary (1951–2001) evolution of lakes in the Old Crow Basin, northern Yukon, Canada: remote sensing, numerical modeling, and stable isotope analysis. *Arctic,* 62: 225–238.

Lajeunesse, P., and St-Onge, G., 2008: The subglacial origin of the lake Agassiz-Ojibway final outburst flood. *Nature Geoscience,* 1: 184–188.

Lamoureux, S. F., 2005: A sediment accumulation sensor for use in lacustrine and marine sedimentation studies. *Geomorphology,* 68: 17–23.

Laurion, I., Vincent, W. F., MacIntyre, S., Retamal, L., Dupont, C., Francus, P., and Pienitz, R., 2010: Variability in greenhouse gas emissions from permafrost thaw ponds. *Limnology and Oceanography,* 55: 115–133.

Lavoie, C., Allard, M., and Duhamel, D., 2012: Deglaciation landforms and C-14 chronology of the Lac Guillaume–Delisle area, eastern Hudson Bay: a report on field evidence. *Geomorphology,* 159-160: 142–155.

Liblik, L. K., Moore, T. R., Bubier, J. L., and Robinson, S. D., 1997: Methane emissions from wetlands in the zone of discontinuous

permafrost: Fort Simpson, Northwest Territories, Canada. *Global Biogeochemical Cycles,* 11: 485–494.

Luoto, M., and Seppälä, M., 2003: Thermokarst ponds as indicators of the former distribution of palsas in Finnish Lapland. *Permafrost and Periglacial Processes,* 14: 19–27.

Matthews, J. A., Dahl, S. O., Berrisford, M. S., and Nesje, A., 1997: Cyclic development and thermokarstic degradation of palsas in the mid-Alpine zone at Leirpullan, Dovrefjell, southern Norway. *Permafrost and Periglacial Processes,* 8: 107–122.

McLaren, J. W., Methven, B. A. J., Lam, J. W. H., and Berman, S. S., 1995: The use of inductively coupled plasma mass spectrometry in the production of environmental certified materials. *Mikrochimica Acta,* 119: 287–295.

Negandhi, K., Laurion, I., Whiticar, M. J., Galand, P. E., Xu, X., and Lovejoy, C., 2013: Small thaw ponds: an unaccounted source of methane in the Canadian High Arctic. *PLoS ONE*, 8(11): e78204, doi: http://dx.doi.org/10.1371/journal.pone.0078204.

Osterkamp, T. E., 2007: Characteristics of the recent warming of permafrost in Alaska. *Journal of Geophysical Research–Earth Surface,* 112: F02S02, doi: http://dx.doi.org/10.1029/2006JF000578.

Parsekian, A. D., Jones, B. M., Jones, M., Grosse, G., Walter, K. M., and Slater, L., 2011: Expansion rate and geometry of floating vegetation mats on the margins of thermokarst lakes, northern Seward Peninsula, Alaska, USA. *Earth Surface Processes and Landforms,* 36: 1889–1897.

Payette, S., 2001: Les processus et les formes périglaciaires. *In* Payette, S., and Rochefort, L. (eds.), *Écologie des tourbières du Québec-Labrador*. Québec: Les Presses de l'Université Laval, 199–240.

Payette, S., and Bouchard, A., 2001: Le contexte physique et biogéographique. *In* Payette, S., and Rochefort, L. (eds.), *Écologie des tourbières du Québec-Labrador*. Québec: Les Presses de l'Université Laval, 9–38.

Payette, S., Delwaide, A., Caccianiga, M., and Beauchemin, M., 2004: Accelerated thawing of subarctic peatland permafrost over the last 50 years. *Geophysical Research Letters,* 31: L18208, doi: http://dx.doi.org/10.1029/2004GL020358.

Pienitz, R., Doran, P. T., and Lamoureux, S. F., 2008: Origin and geomorphology of lakes in the polar regions. *In* Vincent, W., and Laybourn-Parry, J. (eds.), *Polar Lakes and Rivers: Limnology of Arctic and Antarctic Aquatic Ecosystems*. Oxford, U.K.: Oxford University Press, 25–41.

Pissart, A., 2002: Palsas, lithalsas and remnants of these periglacial mounds. A progress report. *Progress in Physical Geography,* 26: 605–621.

Plug, L. J., Walls, C., and Scott, B. M., 2008: Tundra lake changes from 1978 to 2001 on the Tuktoyaktuk Peninsula, western Canadian Arctic. *Geophysical Research Letters,* 35: L03502, doi: http://dx.doi.org/10.1029/2007GL032303.

Pokrovsky, O. S., Shirokova, L. S., Kirpotin, S. N., Audry, S., Viers, J., and Dupré, B., 2011: Effect of permafrost thawing on organic carbon and trace element colloidal speciation in the thermokarst lakes of western Siberia. *Biogeosciences,* 8: 565–583.

Riordan, B., Verbyla, D., and McGuire, A. D., 2006: Shrinking ponds in subarctic Alaska based on 1950–2002 remotely sensed images. *Journal of Geophysical Research–Biogeosciences,* 111: G04002, doi: http://dx.doi.org/10.1029/2005JG000150.

Ropars, P., and Boudreau, S., 2012: Shrub expansion at the forest-tundra ecotone: spatial heterogeneity linked to local topography. *Environmental Research Letters,* 7: 015501, doi: http://dx.doi.org/10.1088/1748-9326/7/1/015501.

Rossi, P.-G., Laurion, I., and Lovejoy, C., 2013: Distribution and identity of bacteria in subarctic permafrost thaw ponds. *Aquatic Microbial Ecology*, 69: 231–245.

Sannel, A. B. K., and Brown, I. A., 2010: High-resolution remote sensing identification of thermokarst lake dynamics in a subarctic peat plateau complex. *Canadian Journal of Remote Sensing,* 36: S26–S40.

Sannel, A. B. K., and Kuhry, P., 2011: Warming-induced destabilization of peat plateau/thermokarst lake complexes. *Journal of Geophysical Research–Biogeosciences,* 116: G03035, doi: http://dx.doi.org/10.1029/2010JG001635.

Saulnier-Talbot, E., and Pienitz, R., 2001: Postglacial isolation of a coastal basin near Kuujjuaraapik-Whapmagoostui, Hudsonie: a diatom biostratigraphical investigation. *Géographie physique et Quaternaire,* 55: 63–74.

Schuur, E. A. G., Bockheim, J. G., Canadell, J. G., Euskirchen, E., Field, C. B., Goryachkin, S. V., Hagemann, S., Kuhry, P., Lafleur, P. M., Lee, H., Mazhitova, G., Nelson, F. E., Rinke, A., Romanovsky, V. E., Shiklomanov, N., Tarnocai, C., Venevsky, S., Vogel, J. G., and Zimov, S. A., 2008: Vulnerability of permafrost carbon to climate change: implications for the global carbon cycle. *BioScience,* 58: 701–714.

Schuur, E. A. G., Vogel, J. G., Crummer, K. G., Lee, H., Sickman, J. O., and Osterkamp, T. E., 2009: The effect of permafrost thaw on old carbon release and net carbon exchange from tundra. *Nature,* 459: 556–559.

Shirokova, L. S., Pokrovsky, O. S., Kirpotin, S. N., and Dupré, B., 2009: Heterotrophic bacterio-plankton in thawed lakes of the northern part of Western Siberia controls the CO_2 flux to the atmosphere. *International Journal of Environmental Studies,* 66: 433–445.

Smith, L. C., Sheng, Y., MacDonald, G. M., and Hinzman, L. D., 2005: Disappearing Arctic lakes. *Science,* 308: 1429.

Smith, L. C., Sheng, Y. W., and MacDonald, G. M., 2007: A first pan-Arctic assessment of the influence of glaciation, permafrost, topography and peatlands on northern hemisphere lake distribution. *Permafrost and Periglacial Processes,* 18: 201–208.

Sokal, R. R., and Rohlf, F. J., 1995: *Biometry: the principles and practice of statistics in biological research*. 3rd edition. New York: W.H. Freeman, 880 pp.

Takakai, F., Desyatkin, A. R., Lopez, C. M. L., Fedorov, A. N., Desyatkin, R. V., and Hatano, R., 2008: CH_4 and N_2O emissions from a forest-alas ecosystem in the permafrost taiga forest region, Eastern Siberia, Russia. *Journal of Geophysical Research–Biogeosciences,* 113: G02002, doi: http://dx.doi.org/10.1029/2007JG000521.

Tarnocai, C., Canadell, J. G., Schuur, E. A. G., Kuhry, P., Mazhitova, G., and Zimov, S., 2009: Soil organic carbon pools in the northern circumpolar permafrost region. *Global Biogeochemical Cycles,* 23: GB2023, doi: http://dx.doi.org/10.1029/2008GB003327.

Tremblay, B., Levesque, E., and Boudreau, S., 2012: Recent expansion of erect shrubs in the Low Arctic: evidence from Eastern Nunavik. *Environmental Research Letters,* 7: 035501, doi: http://dx.doi.org/10.1088/1748-9326/7/3/035501.

Vallée, S., and Payette, S., 2007: Collapse of permafrost mounds along a subarctic river over the last 100 years (northern Quebec). *Geomorphology,* 90: 162–170.

van Huissteden, J., Berrittella, C., Parmentier, F. J. W., Mi, Y., Maximov, T. C., and Dolman, A. J., 2011: Methane emissions from permafrost thaw lakes limited by lake drainage. *Nature Climate Change,* 1: 119–123.

Walter, K. M., Zimov, S. A., Chanton, J. P., Verbyla, D., and Chapin, F. S., 2006: Methane bubbling from Siberian thaw lakes as a positive feedback to climate warming. *Nature,* 443: 71–75.

Walter, K. M., Edwards, M. E., Grosse, G., Zimov, S. A., and Chapin, F. S., 2007: Thermokarst lakes as a source of atmospheric CH_4 during the last deglaciation. *Science,* 318: 633–636.

Walter, K. M., Chanton, J. P., Chapin, F. S., Schuur, E. A. G., and Zimov, S. A., 2008: Methane production and bubble emissions from arctic lakes: isotopic implications for source pathways and ages. *Journal of Geophysical Research–Biogeosciences,* 113: doi: http://dx.doi.org/10.1029/2007JG000569.

Watanabe, S., Laurion, I., Pienitz, R., Chokmani, K., and Vincent, W. F., 2011: Optical diversity of thaw ponds in discontinuous permafrost: a model system for water color analysis *Journal of Geophysical Research–Biogeosciences,* 116: G02003, doi: http://dx.doi.org/10.1029/2010JG001380.

Wickland, K. P., Striegl, R. G., Neff, J. C., and Sachs, T., 2006: Effects of permafrost melting on CO_2 and CH_4 exchange of a poorly drained black spruce lowland. *Journal of Geophysical Research–Biogeosciences,* 111: G02011, doi: http://dx/doi. org/10.1029/2005JG000099.

Wolfe, A. P., Miller, G. H., Olsen, C. A., Forman, S. L., Doran, P. T., Holmgren, S. U., Smol, J. P., Pienitz, R., and Douglas, M. S. V., 2004: Geochronology of high latitude lake sediments. *In* Pienitz, R., Douglas, M., and Smol, J. (eds.), *Long-term Environmental Change in Arctic and Antarctic Lakes*. Dordrecht: Springer, 19–52.

Yoshikawa, K., and Hinzman, L. D., 2003: Shrinking thermokarst ponds and groundwater dynamics in discontinuous permafrost near council, Alaska. *Permafrost and Periglacial Processes,* 14: 151–160.

Zimov, S. A., Schuur, E. A. G., and Chapin, F. S., 2006: Permafrost and the global carbon budget. *Science,* 312: 1612–1613.

Zuidhoff, F. S., and Kolstrup, E., 2000: Changes in palsa distribution in relation to climate change in Laivadalen, northern Sweden, especially 1960–1997. *Permafrost and Periglacial Processes,* 11: 55–69.

APPENDIX

TABLE A1

Detailed results of inductively coupled plasma (ICP) spectrometry measurements.

Sample	Al (µmol g⁻¹)	Ba (µmol g⁻¹)	Ca (µmol g⁻¹)	Fe (µmol g⁻¹)	K (µmol g⁻¹)	Mg (µmol g⁻¹)	Mn (µmol g⁻¹)	Na (µmol g⁻¹)	P (µmol g⁻¹)	S (µmol g⁻¹)	Ti (µmol g⁻¹)	Zn (µmol g⁻¹)	Mo (nmol g⁻¹)	Ag (nmol g⁻¹)	Cd (nmol g⁻¹)	Pb (nmol g⁻¹)	U (nmol g⁻¹)
K2 trap	1425.84	2.91	351.48	1479.39	307.75	321.15	6.28	461.92	311.38	190.18	30.91	1.93	14.51	1.64	4.67	110.74	6.89
K2 surf sed	2732.99	5.12	461.00	755.53	647.83	727.81	10.10	1055.56	31.99	13.58	67.87	1.41	10.71	1.13	1.77	113.58	9.15
K6 trap	2649.65	5.01	364.00	1034.46	621.52	588.90	12.21	1041.99	114.08	52.92	56.29	1.50	9.83	1.24	1.92	105.89	7.49
K6 surf sed	1816.93	4.43	348.16	694.42	570.86	609.55	8.92	945.04	27.29	43.17	61.51	1.45	11.86	1.15	3.21	118.72	7.89
K16 trap	1859.61	5.17	407.24	809.67	651.84	675.66	11.53	1092.37	47.39	15.96	68.90	1.52	7.30	1.60	1.66	108.32	7.61
K16 surf sed	2268.42	5.45	455.96	795.36	679.83	748.99	10.15	1161.21	31.97	14.78	67.95	1.64	10.44	1.36	1.60	118.88	8.34

TABLE A2

Detection limit, precision, and accuracy for each detected element (ICP spectrometry).

Element	Detection limit		Precision (%)	Accuracy (%)
Al	2	μmol g^{-1}	5	5
Ba	0.05	μmol g^{-1}	5	
Ca	5	μmol g^{-1}	10	5
Fe	2	μmol g^{-1}	2	2
K	1	μmol g^{-1}	2	1
Mg	2.5	μmol g^{-1}	2	1
Mn	1	μmol g^{-1}	10	5
Na	5	μmol g^{-1}	5	10
P	2	μmol g^{-1}	5	10
S	2	μmol g^{-1}	5	10
Ti	0.2	μmol g^{-1}	5	10
Zn	0.2	μmol g^{-1}	10	10
Mo	0.5	nmol g^{-1}	5	2
Ag	0.2	nmol g^{-1}	10	10
Cd	0.1	nmol g^{-1}	5	20
Pb	0.5	nmol g^{-1}	10	5
U	0.01	nmol g^{-1}	5	20

TABLE A3

Pearson correlation matrix of selected limnological properties, landscape mapping results, and geochemical measurements in sampled ponds (n = 6). Correlation coefficients (r) discussed in the text are underlined (with their corresponding significant p-values: * = $p < 0.01$; ** = $p < 0.02$; *** = $p < 0.05$).

	DOC	TSS	DOC/TSS	a320	CO2-1	CO2-2	CH4-1	CH4-2	Cond	Oxy	pH	Sal	Dist hill	Dist creek	Area 1959	Area 2006	Area diff	LOI trap	LOI sediment	LOI ridge	LOI trap/sed	LOI trap/ridge	LOI sed/ridge	DI-DOC
DOC	1																							
TSS	0.68	1																						
DOC/TSS	-0.29	-0.81	1																					
a320	0.99	0.64	-0.27	1																				
CO2-1	-0.61	-0.83	0.66	-0.55	1																			
CO2-2	-0.48	-0.82	0.75	-0.41	0.96	1																		
CH4-1	0.54	0.40	-0.44	0.49	-0.45	-0.56	1																	
CH4-2	0.49	0.35	-0.41	0.44	-0.38	-0.50	1.00	1																
Cond	-0.10	0.48	-0.77	-0.16	-0.60	-0.78	0.47	0.46	1															
Oxy	0.26	0.26	-0.44	0.28	-0.63	-0.59	0.39	0.31	0.48	1														
pH	0.60	0.52	-0.41	0.52	-0.62	-0.71	0.94	0.92	0.51	0.33	1													
Sal	-0.36	0.32	-0.68	-0.42	-0.37	-0.58	0.25	0.26	0.95	0.25	0.29	1												
Dist hill	-0.30	0.41	-0.65	-0.37	-0.51	-0.67	0.13	0.13	*0.92	0.28	0.25	0.96	1											
Dist creek	-0.33	-0.06	0.09	-0.29	0.03	0.17	-0.88	-0.92	-0.21	0.01	-0.79	-0.08	0.09	1										
Area 1959	0.47	0.26	-0.12	0.39	-0.35	-0.46	0.88	0.88	0.32	0.09	0.94	0.14	0.08	-0.89	1									
Area 2006	0.22	0.15	-0.06	0.13	-0.23	-0.38	0.75	0.77	0.37	-0.11	0.84	0.29	0.22	-0.84	0.95	1								
Area diff	-0.81	-0.34	0.18	-0.85	0.43	0.28	-0.49	-0.43	0.15	-0.61	-0.40	0.44	0.44	0.25	-0.25	0.06	1							
LOI trap	-0.18	-0.70	0.79	-0.15	0.86	0.87	-0.19	-0.13	-0.78	-0.68	-0.30	-0.67	-0.78	-0.25	0.01	0.05	0.14	1						
LOI sediment	-0.37	-0.48	0.71	-0.43	0.51	0.48	-0.36	-0.30	-0.40	-0.80	-0.20	-0.22	-0.17	-0.02	0.10	0.32	0.66	0.62	1					
LOI ridge	0.34	0.21	0.01	0.38	0.31	0.37	-0.14	-0.10	-0.54	-0.64	-0.19	-0.47	-0.52	-0.04	-0.15	-0.17	-0.08	0.46	0.13	1				
LOI trap/sed	-0.01	-0.64	0.68	0.04	0.75	0.77	0.05	0.11	-0.72	-0.43	-0.12	-0.69	***-0.84	-0.42	0.14	0.10	-0.14	0.94	0.35	0.40	1			
LOI trap/ridge	-0.63	-0.91	0.77	-0.62	0.54	0.52	-0.27	-0.25	-0.25	-0.03	-0.30	-0.16	-0.19	0.04	-0.07	0.03	0.31	0.45	0.47	-0.56	0.40	1		
LOI sed/ridge	-0.77	-0.38	0.04	-0.81	0.03	-0.10	-0.22	-0.21	0.52	0.24	-0.17	0.63	0.65	0.25	-0.16	0.02	0.58	-0.32	0.14	-0.83	-0.41	0.60	1	
DI-DOC	**0.88	0.50	-0.10	0.89	-0.22	-0.12	0.43	0.42	-0.35	-0.17	0.44	-0.52	-0.52	-0.42	0.43	0.24	-0.61	0.21	-0.10	0.69	0.32	-0.61	*-0.95	1

Significant p–values:
p < 0.01 *
p < 0.02 **
p < 0.05 ***

DATA

| Pond #	DOC	TSS	DOC/TSS	a320	CO2-1	CO2-2	CH4-1	CH4-2	Cond	Oxy	pH	Sal	Dist hill	Dist creek	Area 1959	Area 2006	Area diff	LOI trap	LOI sediment	LOI ridge	LOI trap/sed	LOI trap/ridge	LOI sed/ridge	DI-DOC
K1	7.61875	6.26	1.21705	32.6985	1099	1195	255	256	46	9.6	6.63	0.24	30.1385	77.8527	494.291	388.965	-105.33	39.322	6.48536	4.91867	6.0632	7.99444	1.31852	7.2697
K2	5.9075	2.78689	2.11975	21.1035	1680	1686	164	175	38	8.06	6.31	0.24	34.1682	90.4335	469.494	470.402	0.90778	69.3239	10.1292	8.88949	6.84395	7.79841	1.13946	7.3125
K6	3.8025	3.74707	1.01479	8.33501	1095	1024	151	151	61	9.24	6.26	0.33	125.474	141.77	369.093	384.489	15.3955	15.6415	8.22583	1.48599	1.90151	10.5259	5.53557	6.0095
K12	6.9475	2.52	2.75694	27.1748	1013	1274	126	115	36	9.07	6.28	0.21	32.4455	152.024	416.904	364.93	-51.974	41.9202	9.33366	3.66341	4.49129	11.4429	2.54781	6.98524
K16	8.735	24.3048	0.35939	35.656	295	297	295	297	61	9.25	7.24	0.3	103.76	63.253	694.192	635.643	-58.549	10.1562	8.03815	4.30414	2.09504	3.91258	1.86754	7.48799
K20	7.7075	22.1628	0.34777	32.6772	724	919	129	119	47	9.08	6.17	0.26	71.5675	174.901	277.556	221.421	-56.135	12.3478	6.95736	7.95724	1.77479	1.55177	0.87434	7.3115
mean	6.78646	10.2969	1.30262	26.2742	984.333	1065.83	186.667	185.5	48.1667	9.05	6.48167	0.26333	66.259	116.706	453.588	410.975	-42.613	31.4519	8.19493	5.20316	3.86163	7.20434	2.21387	7.06274
median	7.28313	5.00354	1.11592	29.926	1054	1109.5	157.5	163	46.5	9.16	6.295	0.25	52.8679	116.102	443.199	386.727	-54.054	27.4818	8.13199	4.61141	3.29317	7.89643	1.59303	7.2906
max	8.735	24.3048	2.75694	35.656	1680	1686	295	297	61	9.6	7.24	0.33	125.474	174.901	694.192	635.643	15.3955	69.3239	10.1292	8.88949	6.84395	11.4429	5.53557	7.48799
min	3.8025	2.52	0.34777	8.33501	295	297	126	115	36	8.06	6.17	0.21	30.1385	63.253	277.556	221.421	-105.33	10.1562	6.48536	1.48599	1.77479	1.55177	0.87434	6.0095
SD	1.73438	10.1301	0.96689	10.1946	458.939	460.226	70.9892	74.9607	10.8336	0.52154	0.40336	0.04412	41.0336	45.4296	140.906	136.561	44.0826	23.1268	1.37971	2.76591	2.25634	3.81479	1.73294	0.54097
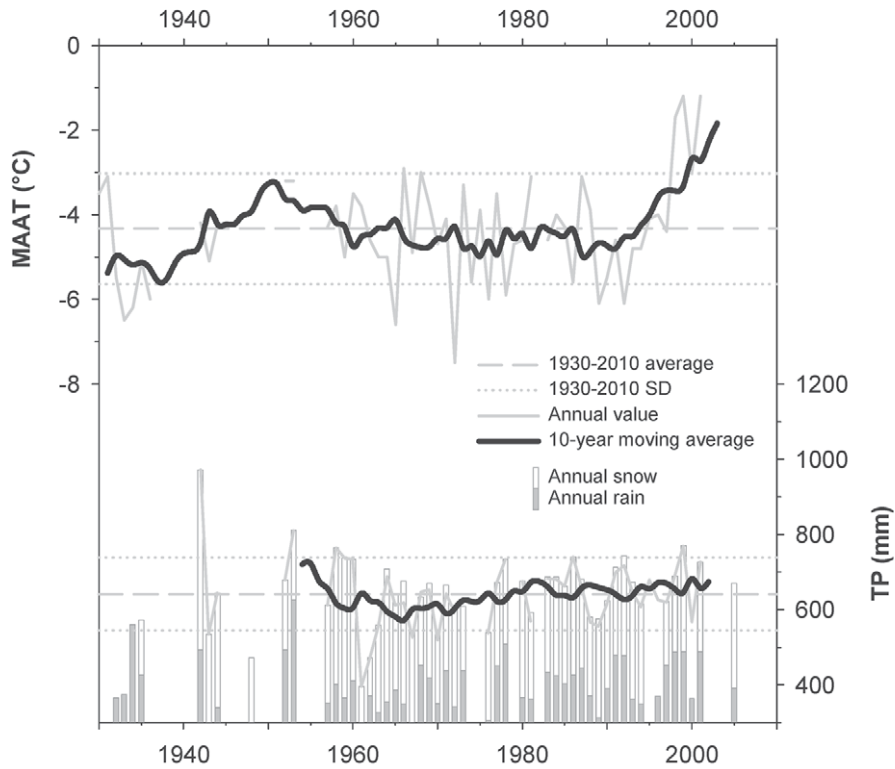
FIGURE A1. Mean annual air temperature (MAAT, upper graph) and total annual precipitation (TP, lower graph) at the Kuujjuarapik-Whapmagoostui weather station between 1930 and 2010 (Environment Canada, 2012b). Long-term average (dashed line), standard deviation (dotted line), annual value (thin gray line) and 10-year moving average (thick black line) are shown. Proportion of rain (gray bars) and snow (open bars) are also included.
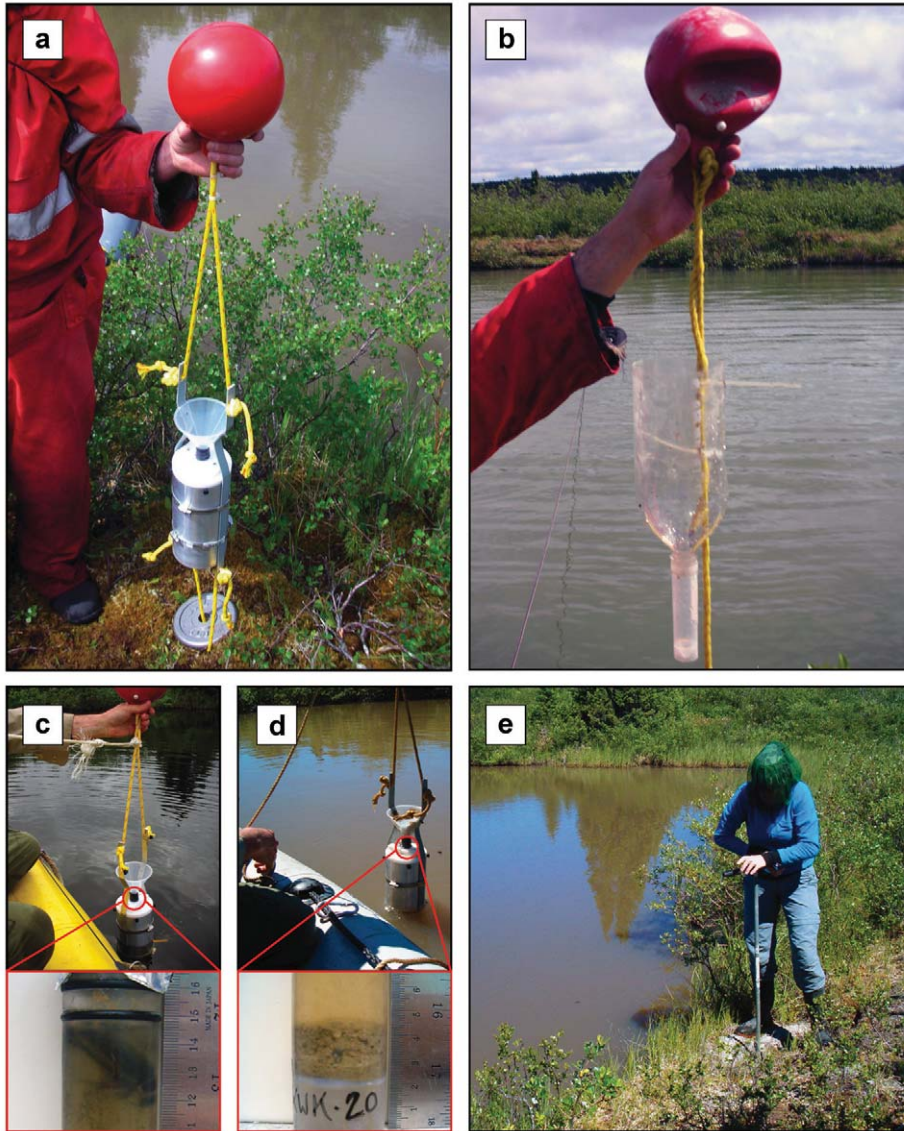
FIGURE A2. Sediment trap and soil sampling methods in July 2007 and July 2008. (a) Sediment flux sensor ("active trap") equipped with an optical system and a datalogger. (b) Homemade ("passive") sediment trap. (c) Sediment flux sensor in humic/black-colored pond K12 (enlargement: accumulation vessel partially blocked by a large aquatic insect (Coleoptera, genus *Dytiscus*). (d) Sediment flux sensor in turbid/beige-colored pond K20 (enlargement: sediments accumulated between 2007 and 2008). (e) Soil sampling in peripheral ridge of pond K1 (brown color).
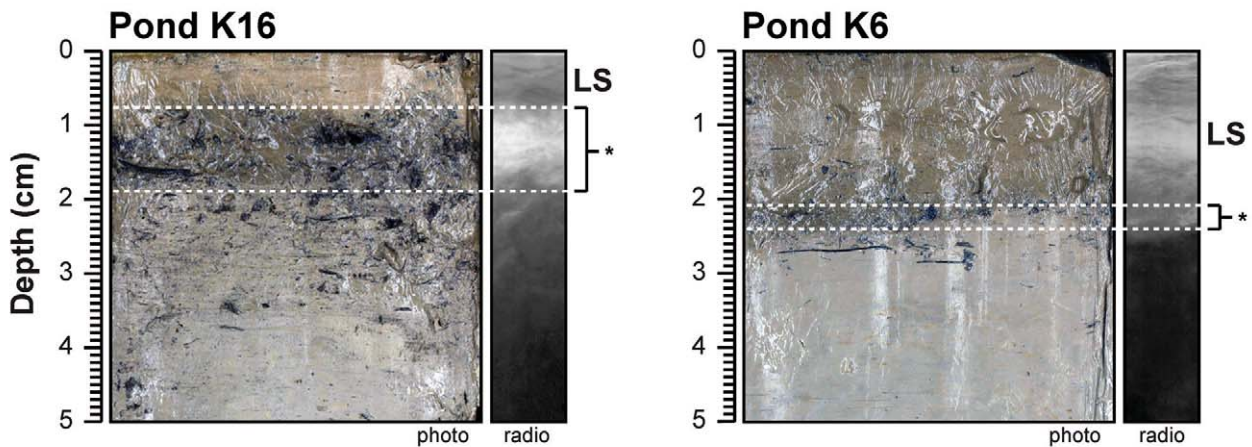

FIGURE A3. Combined photographs and x-radiographs of sediment cores taken in pond K16 (left) and K6 (right), showing thickness and depth of peat layers (*) underlying recent lacustrine sediments (LS).